British Geological Survey
NATURAL ENVIRONMENT RESEARCH COUNCIL

Detection of fracture dilatancy on the cliff top using the azimuthal apparent resistivity technique

Coastal Geoscience & Global Change Impacts Programme

Internal Report IR/04/20

BRITISH GEOLOGICAL SURVEY

INTERNAL REPORT IR/04/20

Detection of fracture dilatancy on the cliff top using the azimuthal apparent resistivity technique

J P Busby, M G Raines, P D Jackson, L Nelder and D J R Morgan

The National Grid and other Ordnance Survey data are used with the permission of the Controller of Her Majesty's Stationery Office. Ordnance Survey licence number GD 272191/1999

Key words

Cliff collapse, prediction, azimuthal resistivity.

Front cover

Cliff collapse at the Birling Gap research site on 9th January 2003.

Bibliographical reference

BUSBY, J P, RAINES, M G, JACKSON, P D, NELDER, L AND MORGAN, D J R. 2004. Detection of fracture dilatancy on the cliff top using the azimuthal apparent resistivity technique. *British Geological Survey Internal Report*, IR/04/20. 42pp.

© *NERC 2004*

Keyworth, Nottingham British Geological Survey 2004

BRITISH GEOLOGICAL SURVEY

The full range of Survey publications is available from the BGS Sales Desks at Nottingham and Edinburgh; see contact details below or shop online at www.thebgs.co.uk

The London Information Office maintains a reference collection of BGS publications including maps for consultation.

The Survey publishes an annual catalogue of its maps and other publications; this catalogue is available from any of the BGS Sales Desks.

The British Geological Survey carries out the geological survey of Great Britain and Northern Ireland (the latter as an agency service for the government of Northern Ireland), and of the surrounding continental shelf, as well as its basic research projects. It also undertakes programmes of British technical aid in geology in developing countries as arranged by the Department for International Development and other agencies.

The British Geological Survey is a component body of the Natural Environment Research Council.

Keyworth, Nottingham NG12 5GG

☎ 0115-936 3241 Fax 0115-936 3488
e-mail: sales@bgs.ac.uk
www.bgs.ac.uk
Shop online at: www.thebgs.co.uk

Murchison House, West Mains Road, Edinburgh EH9 3LA

☎ 0131-667 1000 Fax 0131-668 2683
e-mail: scotsales@bgs.ac.uk

London Information Office at the Natural History Museum (Earth Galleries), Exhibition Road, South Kensington, London SW7 2DE

☎ 020-7589 4090 Fax 020-7584 8270
☎ 020-7942 5344/45 email: bgslondon@bgs.ac.uk

Forde House, Park Five Business Centre, Harrier Way, Sowton, Exeter, Devon EX2 7HU

☎ 01392-445271 Fax 01392-445371

Geological Survey of Northern Ireland, 20 College Gardens, Belfast BT9 6BS

☎ 028-9066 6595 Fax 028-9066 2835

Maclean Building, Crowmarsh Gifford, Wallingford, Oxfordshire OX10 8BB

☎ 01491-838800 Fax 01491-692345

Parent Body

Natural Environment Research Council, Polaris House, North Star Avenue, Swindon, Wiltshire SN2 1EU

☎ 01793-411500 Fax 01793-411501
www.nerc.ac.uk

Foreword

This report is a detailed account of the azimuthal apparent resistivity data collected by the BGS over a period of two years in order to investigate the possibility of detecting time dependant fracture dilatancy. Such dilatancy is expected to occur within sea cliffs composed of fractured rock. If successful, the methodology might be adaptable as a technique for providing an early warning of impending cliff failure. The investigation formed a work package of the co-funded project 'PROTECT' (PRediction Of The Erosion of Cliffed Terrains). This project was supported by the EU 5th Framework research and development programme.

Acknowledgements

The data in this report were collected at five research sites, distributed between the East Sussex coast of the UK, the Normandy coast of France and the Baltic coast of Denmark. Generous help was provided by colleagues in the PROTECT consortium in establishing the sites and in collecting the subsequent field data. PROTECT consortium members also provided other data sets that have contributed to the interpretation of the data presented here. The authors would like to thank in particular:

Mr James Lawrence (University of Brighton)

Professor Rory Mortimore (University of Brighton)

Mr Jean Christophe Gourry (Bureau de Recherche Géologiques et Minières)

Dr Stig Pedersen (Geological Survey of Denmark and Greenland)

Mr Lasse Gudmundsson (Geological Survey of Denmark and Greenland)

Dr Ingelise Møller (Geological Survey of Denmark and Greenland)

Thanks are also due to Dave Pearce of Eastbourne Borough Council, Glenn Redman of the National Trust, H. Gravesen of the Danish Agency of Natural Preservation and Forestry and the Mayor of Mesnil-Val who all assisted with access to the sites.

Contents

FIGURES

TABLES

Summary

Hard rock cliffs erode through an initial catastrophic collapse along pre-existing discontinuities in the rock mass. These may be ancient faults or fractures, orientated at a variety of angles to the cliff face, or relatively new tension fractures formed during cycles of cliff recession, sub-parallel to the cliff face. It is likely that an approaching cliff fall will be associated with increasing fracture dilatancy within the fracture network. Hence if the change of dilatancy can be measured then it may be possible to generate alerts of impending cliff collapse.

Since fractures often occur in sets with a preferred orientation they impose anisotropic physical properties on the rock mass. Hence, the apparent resistivity of the rock will vary with azimuth reflecting the dominant fracture orientation. Measures of anisotropy can be calculated from the measurements and would be expected to vary with time if the fractures are dilating.

Work package one of the 5th Framework co-funded project 'PROTECT' (PRediction Of The Erosion of Cliffed Terrains) was to detect fracture dilatancy. Azimuthal apparent resistivity data were collected at five research sites in the UK, France and Denmark, all situated on outcropping chalk. At each research site, data were collected with the Square array at three locations near the cliff edge and at a Control site set back from the cliff edge by about 50 m. Data were collected approximately every two months for two years to create a temporal data set. After processing the data to remove the effect of the infinite resistance afforded by the cliff face, the data were fitted to an ellipse in order to test for anisotropy. Measures of anisotropy were then calculated from these data.

The anisotropy has been interpreted as fracturing and indicates a number of tectonic fracture orientations that agree with geological mapping. At several of the research sites a cliff-parallel fracture set was identified in a zone 10 to 20 m wide adjacent to the cliff edge. It is assumed that this fracture set develops in response to the stress relief at the cliff face. At the Birling Gap research site a cliff collapse within the zone of resistivity measurements produced a dramatic drop in the magnitude of the post-collapse calculated measures of anisotropy. However, other cliff falls that occurred outside of the immediate zone of resistivity measurements did not generate appreciable changes in the calculated measures of anisotropy. It appears that the tectonic fractures that limit the lateral extent of the cliff fall may also limit the fracture dilatancy within the cliff parallel fracture set. At some sites there was a seasonal variation in the measures of anisotropy with peaks in the summer and troughs in the winter. It appears that the most likely driver for these variations is rock temperature that is itself controlled by the external air temperature.

Overall, the research has been successful in establishing that there are measurable changes in the rock mass prior to a collapse. However, the methodology is not yet advanced enough to be able to develop technology for the reliable early warning of a cliff fall. The next stage of any research would be to install a system for continuous monitoring in order to establish the magnitude of the changes in the measures of anisotropy immediately prior to a cliff collapse.

1 Introduction

Over the years a considerable body of data has been collected on the nature and lithology of coastal cliffs. This has enabled geologists and engineers to develop a better understanding of cliff collapse mechanisms and the factors that determine rates of erosion. However there has been very little research into physical property changes within the rock mass behind a cliff face prior to collapse. If any such changes can be quantified, they could be used as precursors to impending collapse.

A European Union 5th Framework Research and Development project 'PROTECT' (Prediction Of the Erosion of Cliffed Terrains) started in April 2001 to research methods that might generate precursors. In addition, data collected as part of the project will contribute in the development of models of cliff collapses. The PROTECT project is co-ordinated by the British Geological Survey and other partners comprise the University of Brighton (UoB), the Bureau de Recherche Géologiques et Minières (BRGM), the Geological Survey of Denmark and Greenland (GEUS), the Institut National de l'environement Industriel et des Risques (INERIS), the Isle of Wight Centre for the Coastal Environment (IWCCE), the Direction Departementale de L'equipement de la Seine Maritime (DDE76), Urzad Morski w Gdyni (PMA) and Consorzio Ferrara Ricerche (CFR).

This report is an account of the scientific contribution of the British Geological Survey to the project. This has focussed on the application of azimuthal apparent resistivity (AZR) to the coastal cliff top. It is a reasonable assumption that in the upper part of a cliff, sub-vertical fractures within the rock will gradually dilate with time until a collapse is initiated. Since fractures often occur in sets with a preferred orientation they impose anisotropic physical properties on the rock mass. It has been shown that the apparent resistivity of the rock will vary with azimuth reflecting the dominant fracture orientation. Anisotropy factors can be calculated from the measurements that would be expected to vary with time if the fractures are dilating.

In addition to the collection of AZR data, this report also gives an account of the processing developed and applied to the data, an initial interpretation of the results and conclusions that can be drawn about the methodology.

2 Azimuthal resistivity on the coastal cliff top

It is known that fractures in hard rocks such as chalk and limestone occur in parallel sets, which impose anisotropic physical properties on the rock mass. The catastrophic failure of a cliff is likely to occur along one of these sets of fractures, at least in the upper part of the cliff. Increased tension (dilatancy) within the fracture network will increase the anisotropy of the rock mass. Hence, a relative measure of the increased anisotropy will indicate sections of cliff where the fracture tension is increasing. It is highly likely that increased tension within the fracture network will eventually lead to rock failure, although the timing (months or years) is not currently known. However, knowledge of fracture tension will help to identify vulnerable sections of coastline.

An apparent resistivity measurement is made by imposing a low energy direct current between two electrodes implanted into the ground surface. The resultant distribution of ground potential is measured between additional pairs of potential electrodes (see Figure 1). When the resistivity of any material contained within the fractures differs from that of the host rock, the measured apparent resistivity will vary with the orientation of the electrode array. Measurements are made by rotating the electrode array through 180° or 360° and taking measurements along a sufficient number of azimuths to define any variation of apparent resistivity with orientation (Taylor and Fleming 1988). The apparent resistivities (in ohm.m) for each electrode spacing are plotted

against azimuth in a polar diagram. If the plotted figure is circular then either there are no measurable fracture sets or the volume of rock investigated was insufficient because the structure and material sampled were, to the limit of measurement, isotropic. This may well be the case for shallow depths, sampled at short spacings. If an ellipse results then the azimuth of the principal fracture set can be defined. For co-linear arrays, the major axis of the ellipse is coincident with the strike of the fractures, whilst for a square array the minor axis of the ellipse is parallel to the fracture strike. A measure of the anisotropy can be obtained from the ratio of the maximum and minimum apparent resistivities. For a square array, the coefficient of anisotropy, λ is defined as

$$\lambda = \sqrt{\frac{\rho_y}{\rho_x}} = \frac{\rho_{x_{app}}}{\rho_{y_{app}}}$$

where ρ_y is the true resistivity parallel to the fractures, ρ_x is the true resistivity normal to the fractures, $\rho_{x_{app}}$ is the apparent resistivity normal to the fractures and $\rho_{y_{app}}$ is the apparent resistivity parallel to the fractures.

If the measurements are repeated over a period of time, any variations indicate an alteration of the physical properties of the rock mass, one of which could be changes in dilatancy within the fracture network.

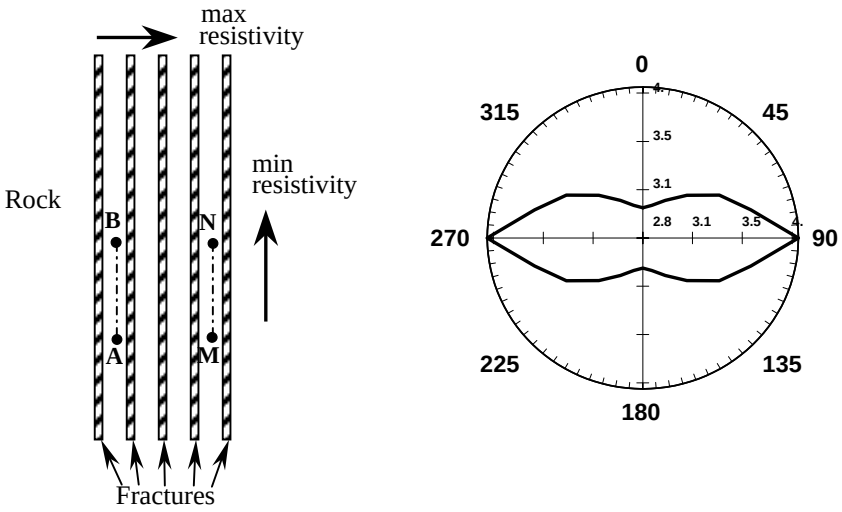

Figure 1. A set of parallel fractures will impose anisotropy on an apparent resistivity measurement, conducted through current electrodes A, B and potential electrodes M, N. When the electrodes are rotated about the centre of the square A, B, M, N and the results plotted against azimuth in a polar diagram, an ellipse results. The major axis of the ellipse is perpendicular to the fracture strike.

2.1 ELECTRODE CONFIGURATION

The majority of AZR measurements have been taken with the electrodes arranged colinearly (e.g. Nunn *et al*. 1983, Busby 2000). On a cliff top, space is restricted, so it may be more appropriate to consider a non-linear array. Three different electrode arrays were trialed in order to find the array most sensitive to anisotropy. These comprised the Offset Wenner array (Barker 1981), the Square array (Habberjam and Watkins, 1967) and the Arrow array (Bolshakov et al., 1998). The trial site was located on chalk at Telscombe Tye on the east Sussex coast of the UK [NG 539.25, 101.65], near Telscombe Cliffs. The square array was the only array to give coherent results that indicated a strike for the chalk fractures. The direction obtained, 15°, is in

agreement with fracture mapping carried out in the Telscombe Tye area (R. Mortimore pers. comm.). A full account of the trial is given in Busby (2001).

Subsequent to the trial described above, the Square array was selected for all the cliff top measurements. Habberjam and Watkins (1967) have shown that with the electrodes arranged in a square they are more sensitive to anisotropy and require about 65% less surface area than an equivalent, rotated, colinear array. Lane *et al*. (1995) have applied the azimuthal square array to the mapping of bedrock fractures and have extended the interpretational analysis. By using a switch box there are three electrode configurations for each square (see Figure 2).

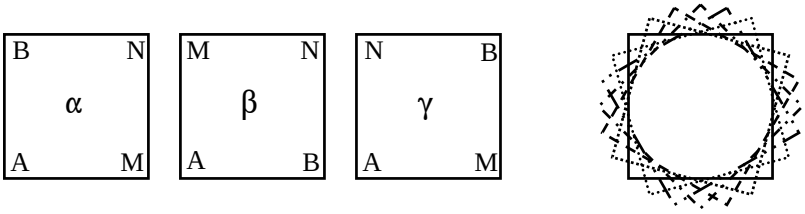

Figure 2. The α, β and γ configurations of the square array where A, B are current electrodes and M, N are potential electrodes. By rotating the array in increments of 15°, all orientations are defined with six configurations.

The α and β configurations are perpendicular measurements. The γ measurement serves as a check on the accuracy of the α and β measurements since in a homogeneous anisotropic medium,

$$\rho_{a\gamma} = \rho_{a\alpha} - \rho_{a\beta}$$

where ρ_a = apparent resistivity in Ω.m. Apparent resistivity is calculated from the measured potential difference (ΔV) and current (I) by the relation;

$$\rho_a = \frac{2\pi a \Delta V}{(2-\sqrt{2})I}$$

where 'a' is the Square array side length in metres. If the square is rotated about its centre point in increments of 15°, it requires only six rotations to define all orientations. The direction of fracture strike occurs perpendicular to the direction of maximum resistivity; the opposite situation to that of co-linear arrays.

The volume of rock involved in the measurement (and hence the number of fractures crossed) as well as the depth of penetration are determined by the array spacing, that is, the length of a side of the square. In practice all array spacings at a particular orientation would be completed before rotating the array.

2.2 MEASUREMENT PROCEDURE

Five sites were chosen, spread between the UK, France and Denmark where, in all cases, the lithology comprised flat lying chalk overlain by very thin drift. Chalk is known to be highly fractured and its permeability arises from the fracturing. On each cliff top, three sites perpendicular to the cliff face were established and a control site was setup approximately 50 m from the cliff (see Figure 3). Those sites near the cliff edge (Sites A, B and C) should sample ground that is likely to be affected by fracture dilatancy. The maximum electrode spacing (side of the square) for the three sites near the cliff face was set so that nearest approach of an electrode to the cliff edge was about one to two metres. Some temporal variations are likely to be observed due to influences such as seasonal changes in saturation levels, but these should also be observed at the Control Site. A time series was built up by repeating the measurements every two months for a period of two years.

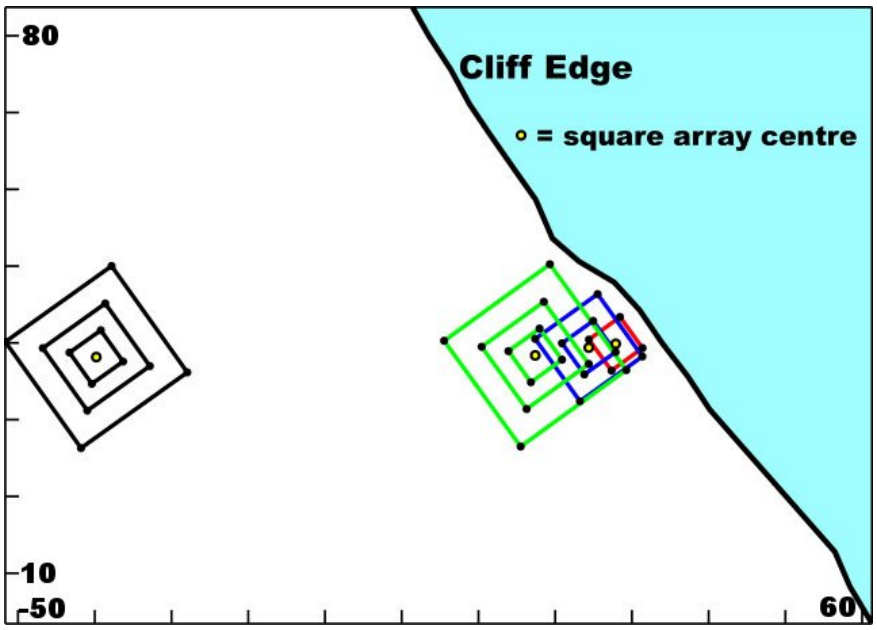

Four centres

Site A: a = 5 m

Site B: a = 5, 10 m

Site C: a = 5, 10, 20 m

Control: a = 5, 10, 20 m

Where 'a' = the side of the square.

For Sites A, B and C the outer electrode approaches to within 1 to 2 m of the cliff edge.

Figure 3. Deployment of the square array on the cliff top with three soundings near the cliff edge and a control sounding set back from the cliff edge.

3 The research sites

Five research sites were established at three localities. These comprised Beachy Head and Birling Gap on the East Sussex coast of the UK. Mesnil-Val on the Normandy coast of France and, Jættebrink and Dronningestolen located at Møns Klint on the island of Møns facing the Baltic Sea off Denmark.

3.1 BEACHY HEAD

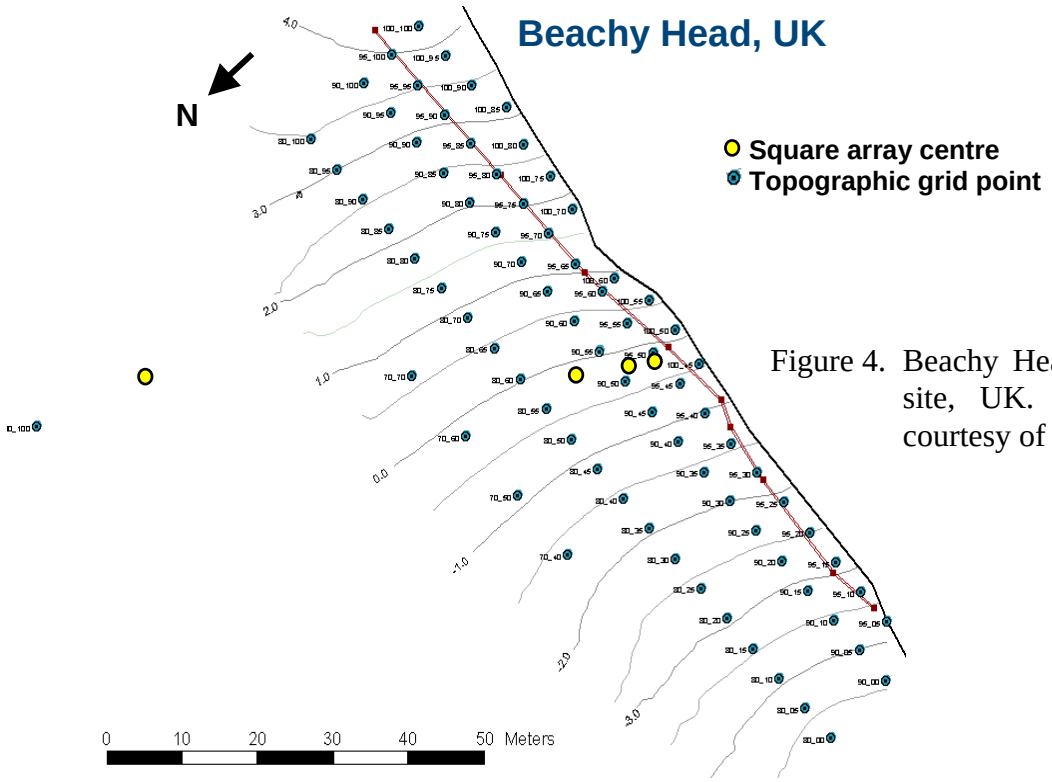

Figure 4. Beachy Head research site, UK. Base map courtesy of GEUS.

Figure 5. Beachy Head Site A, view looking east.

The Beachy Head site is located at British National Grid (km) co-ordinates [558.11E, 95.29N]. The cliff at the Beachy Head site is composed of Seaford Chalk in the upper part of the cliff, underlain by Lewes Nodular Chalk. Seaford Chalk is characterised by sub-vertical fractures with mapped dominant fracture orientations of 70° and 150° (J. Lawrence pers. comm.). The site is on a westerly facing slope that has undergone deep periglacial weathering that might have created randomly orientated fractures near surface and a variety of dissolution features. The site is on the northerly limb of the Beachy Head Anticline and dips at 15° to 20° to the north-west. The site is used very heavily by tourists and as a result the grass is short and there is excellent access at all times. No cliff falls occurred during the two years of measurements.

3.2 BIRLING GAP

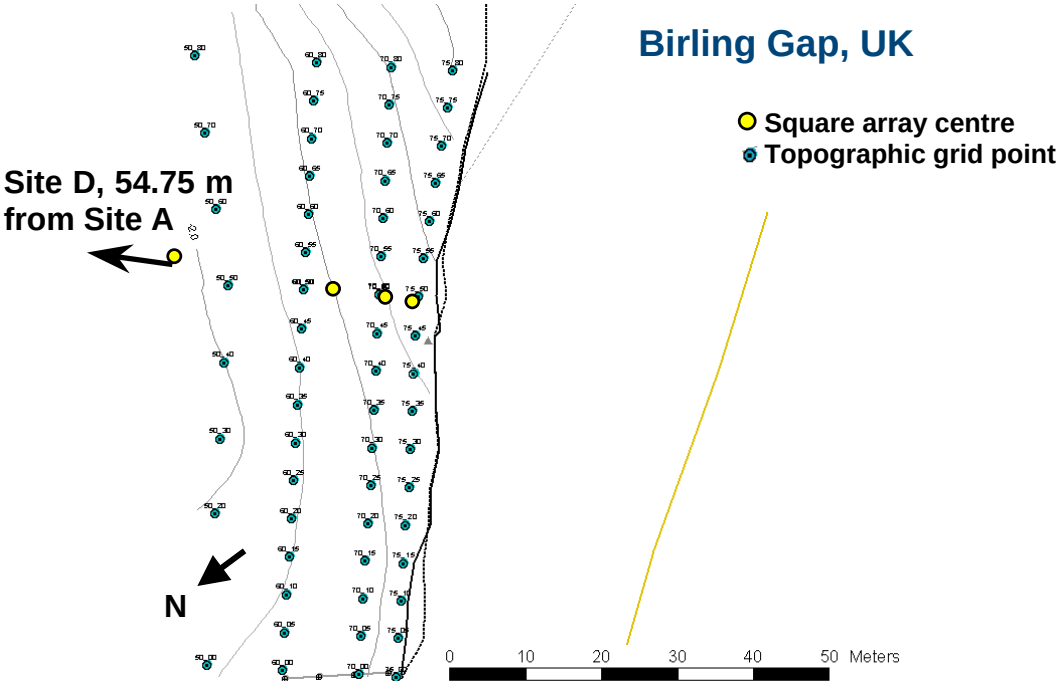

Figure 6. Birling Gap research site, UK. Base map courtesy of GEUS.

Figure 7. Birling Gap Site C, view looking west-north-west.

The Birling Gap site is located at British National Grid (km) co-ordinates [555.65E, 95.73N] and is approximately 2.5 km west from the Beachy Head site. Due to the north-westerly dip of the chalk the Seaford Chalk that is exposed at the top of Beachy Head is found at about 20 m below the top of the cliff at Birling Gap. The entire cliff is composed of Seaford Chalk and is characterised by sub-vertical fracturing. A north-west-trending fault is clearly visible in the wave-cut platform that intersects the cliff at the research site. The strata at Birling Gap are approximately horizontal. Periglacial weathering is less intense than at Beachy Head and there are less dissolution features. The area is owned by the National Trust and is again favoured by short grass and easy access. Two small cliff falls occurred during the project, one between March and May 2002 and the other on 9th January 2003.

3.3 MESNIL-VAL

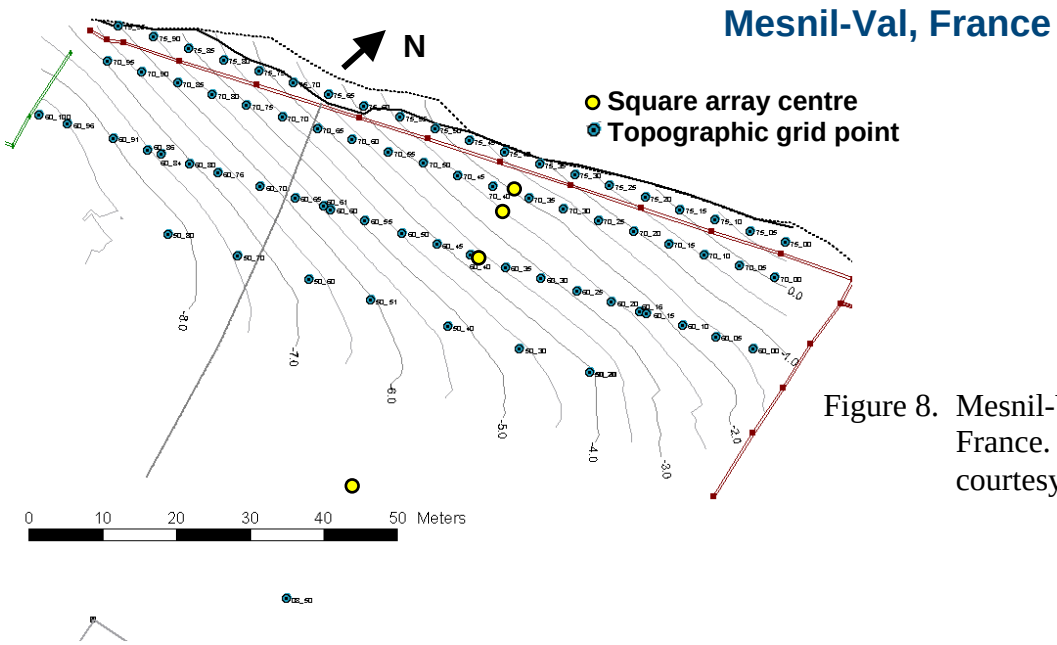

Figure 8. Mesnil-Val research site, France. Base map courtesy of GEUS.

Figure 9. The Mesnil-Val research site, view looking south from the cliff edge.

The Mesnil-Val research site is located at IGN km co-ordinates of [528.2E, 1261.35N]. The cliff is composed of Lewes Nodular Chalk. The fracturing is sub-vertical and two conjugate fracture sets have been mapped striking at 30° and 127°. The south-facing slope of the research site has been subjected to some periglacial weathering. This has resulted in a number of linear cryoturbated lobes filled with silty material that strike at ~150°. Some of the fractures at Mesnil-Val have been observed to be filled with loess. The field at Mesnil-Val was not farmed for the duration of the project and as a result the grass grew very long during the summer. A medium sized cliff fall occurred on June 23rd 2002.

3.4 JÆTTEBRINK

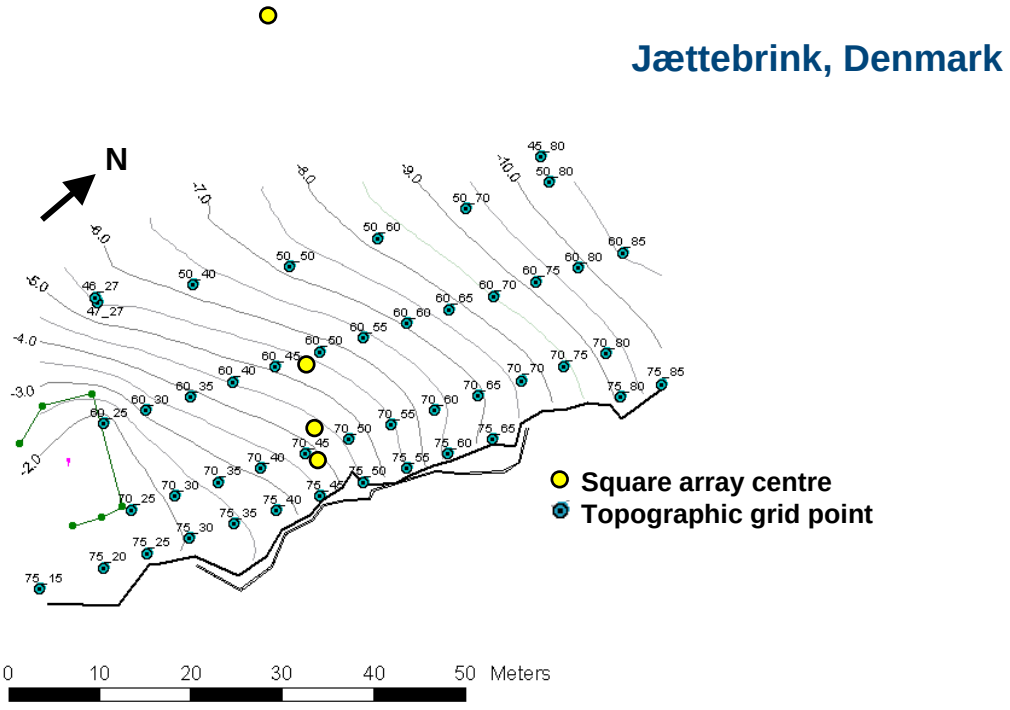

Figure 10. Jættebrink research site, Møns Klint, Denmark. Base map courtesy of GEUS.

Figure 11. Jættebrink Site B, view looking north-north-east.

The Jættebrink research site is located at UTM Zone 33 km co-ordinates of [342.86E, 6092.3N]. The chalk of Møns Klint has been highly deformed by glaciotectonics. The chalk originated from the Baltic and was moved by northerly flowing ice before being deformed again by an ice sheet from the east. As a result, thrust sheets of chalk lie over and are intermingled with slabs of glacial till. The Jættebrink cliff is 25 to 30 m high and contains no till, but a sub-horizontal thrust divides the cliff into an upper and lower section. The glaciotectonics has generated a highly fractured chalk with many fracture sets, but with low persistence and high frequency. No cliff falls occurred during the two years of measurements.

3.5 DRONNINGESTOLEN

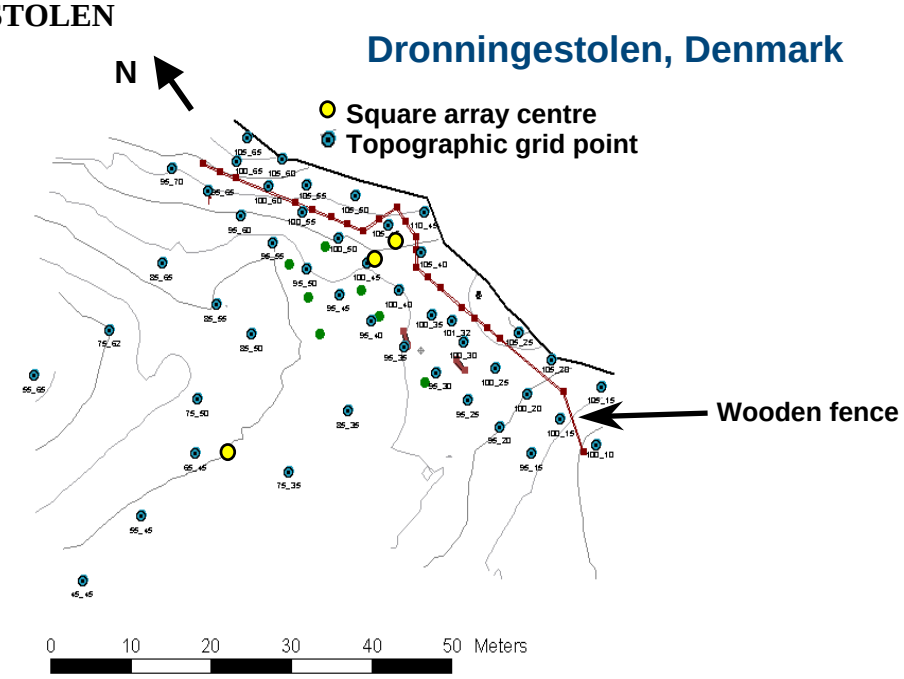

Figure 12. Dronningestolen research site, Møns Klint, Denmark. Note that due to space limitations there is no Site C, only A and B, near the cliff, and a Control. Base map courtesy of GEUS.

Figure 13. Dronningestolen, view looking from the cliff towards the west. The equipment is located at Site B and the yellow marker of Site A can be seen in the foreground.

The Dronningestolen research site is located at UTM Zone 33 km co-ordinates of [343.22E, 6094.14N]. Dronningestolen is situated on the highest peak of the glaciotectonised chalk of Møns Klint at 130 m above sea level. As at Jættebrink there is no till within the cliff. Unlike all the other research sites, the area is wooded and is managed by the Danish Agency of Natural Preservation and Forestry. Lack of space due to the trees resulted in the establishment of only Sites A and B and a Control site. The roots of the trees will alter the moisture distribution within the ground and it was expected that this might have an influence on the azimuthal resistivity measurements. No cliff falls occurred during the two years of measurements.

4 Data collection

A requirement of the data collection was to be able to re-occupy measurement sites accurately and take the measurements efficiently, because in the winter the days are short. This was accomplished by marking the centre of each square array with a permanent ground marker that consisted of a 35 cm steel stake fitted with a stainless steel spring retention lug to prevent the stake from being removed from the ground. To aid relocation, the stake was topped with a yellow survey marker disc (see Figure 14).

Figure 14. Permanent ground marker placed at the centre of each square array. It consisted of a steel stake topped with a yellow survey disc.

From this survey point, an arbitrary compass orientation was selected looking inland, approximately at right angles to the cliff line and was marked with a ranging rod. A further 11 ranging rods were then deployed at 15° increments using the circular scale on an autoset level, levelled over the survey marker. Three were positioned to the left and eight to the right of the initial orientation. Four survey tapes were anchored at the survey marker by a thirteenth ranging rod that screwed into the top of the steel stake. These tapes were deployed along the diagonals of the square to locate the electrode positions.

Data were collected with an ABEM Terrameter 300 C and Booster. For each square, the α, β and γ configurations were selected via a switch box. Since the α and β configurations are perpendicular, it is necessary to rotate the square (i.e. move the survey tapes) only six times in order to measure all orientations. The ranging rod positions were marked with wooden stakes for reoccupation and these were colour coded as white for Site A, yellow for Site B and red for Sites C and the Control. An example of the initial set-up for each square with the positions of the wooden stakes is shown for Jættebrink in Figure 15.

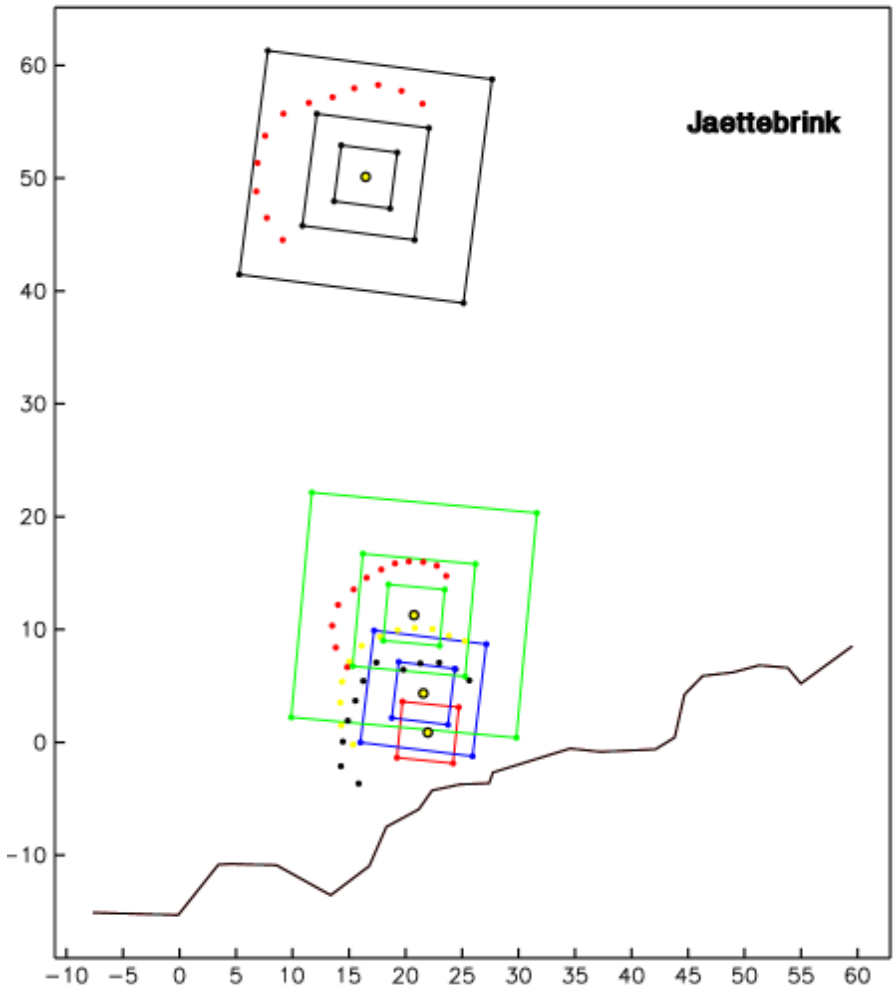

Figure 15. Initial set-up for each square, around its central survey marker, shown for Jættebrink. Site A is shown in red, Site B in blue, Site C in green and the Control Site is in black. Positions of the wooden stakes, for reoccupation of the ranging rods, are shown for each square. Note that the wooden stakes for Site A were white, but are shown here in black.

At each location Site A was established such that during the rotation the electrodes approached to within one to two metres of the cliff edge. Site B was set 3.53 m from Site A and Site C 10.6 m from Site A. The Control Site was approximately 50 m from the cliff. There was no Site C at Dronningestolen due to space limitations. Electrode spacings (side of the square) consisted of 5 m for Site A; 5 and 10 m for Site B; 5, 10 and 20 m for Sites C and the Control. However at Beachy Head, again due to space limitations, the final spacing for Site C and the Control was 17 m. A cliff fall at Birling Gap between the beginning of March and the end of April 2002 required Sites A and B to be moved 1.5 m farther from the cliff and the Site C final spacing to be reduced to 17 m. These changes were implemented from the sixth visit in July 2002.

In all, each research site was visited 12 times, approximately every two months. The exact dates are shown Table 1.

Beachy Head	**Birling Gap**	**Mesnil-Val**	**Jættebrink**	**Dronningestolen**
28th August 2001	27th August 2001	29th August 2001	5th September 2001	4th September 2001
23rd October 2001	22nd October 2001	25th October 2001	10th November 2001	9th November 2001
10th January 2002	10/11th January 2002	8th January 2002	14/15th January 2002	15/16th January 2002
4th March 2002	5th March 2002	7th March 2002	10th March 2002	10th March 2002
22/23rd April 2002	23rd April 2002	25th April 2002	30th April 2002	30th April 2002
1st July 2002	2nd July 2002	4th July 2002	7th July 2002	7th July 2002
2nd September 2002	3rd September 2002	5th September 2002	28th August 2002	28th August 2002
6/7th November 2002	7th November 2002	9th November 2002	12th November 2002	12th November 2002
8th January 2003	9th January 2003	11th January 2003	16th January 2003	17th January 2003
5th March 2003	4th March 2003	7th March 2003	10th March 2003	10th March 2003
28th April 2003	1st May 2003	3rd May 2003	16th May 2003	16th May 2003
23rd June 2003	24th June 2003	26th June 2003	16th July 2003	16th July 2003

Table 1. Dates on which azimuthal apparent resistivity measurements were taken at each of the research sites.

5 Data processing

After reduction of the data to apparent resistivities a number of processing steps were applied. These consisted of:

- A correction for the infinite resistance afforded by the cliff that manifests itself as current focussing toward the cliff edge. This correction is significant because the area of interest is immediately adjacent to the cliff.
- An assessment of data quality of the azimuthal apparent resistivities in order to determine whether anisotropy parameters can be calculated.
- The calculation of a number of derived parameters.

5.1 THE CLIFF CORRECTION

The data need to be corrected for the effect of the cliff edge. The rotated square array measurements were simulated using a 3D finite difference approach (Jackson et al., 2001) incorporating the surveyed cliff co-ordinates at a resolution far in excess of the surveyed points.

From this a correction has been developed for the infinite resistance afforded by the cliff and applied to the data. The modelling approach was to input the actual co-ordinates of the cliff and test whether the resistivity at each node of the forward model should be set to be infinitely large (i.e. air). Angular variations were modelled by rotating the cliff around the nodes of the forward model in 15-degree increments (see Figure 16). This ensures that the parts of the model where the current density is highest are always represented by the same, high-density grid for each rotation.

The correction is significant because the area of interest is immediately adjacent to the cliff. Models have been completed for each site and at Birling Gap separate models were created for the pre- and post- 2002 collapse. The application of the correction generates a reduction in the apparent resistivity measured. Corrections as high as 50% were calculated for the 5 m square array closest to the cliff, compared to the homogeneous case (i.e. no cliff present). Moving away from the cliff, these differences decreased as expected, to a few percent for those arrays that did not expand as far as the cliff edge. At the control sites the corrections were negligible.

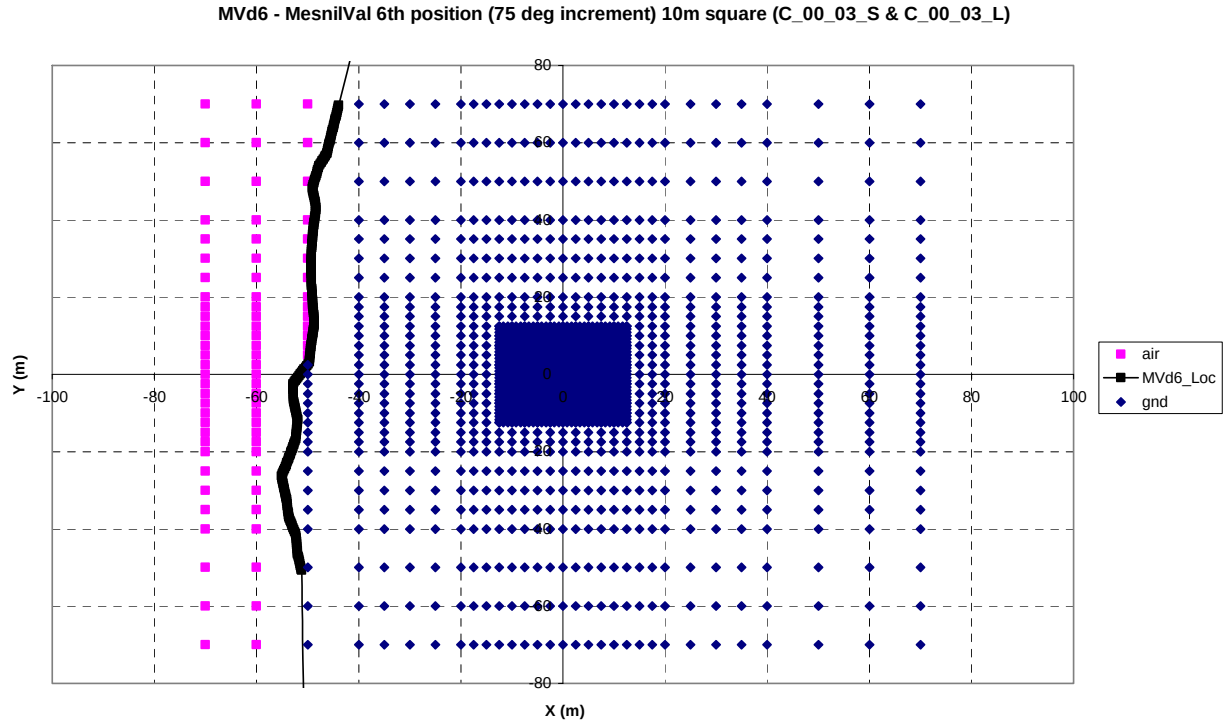

Figure 16. An example of the finite difference model for Mesnil-Val showing the model used to calculate the cliff correction for the 10 m square after a rotation of 75 degrees. The cliff edge is the bold solid line.

5.2 AZIMUTHAL DATA QUALITY

The apparent resistivities obtained for any electrode spacing of an azimuthal set-up (array rotated through 180° or 360°) are subject to geological noise. A measure is needed which defines the goodness of fit to an elliptical model and hence, indicates anisotropy, as compared to a circular model, which indicates isotropy. Hart and Rudman (1997) fit the measured data to a best-fit ellipse. Having obtained the coefficients of the best-fit ellipse, the variance (σ^2) that this ellipse minimised is calculated. This is compared to the variance of the data, which represents the goodness-of-fit to a circular model, to define a statistic R^2, where

$$R^2 = \frac{(\sigma^2_{(circle)} - \sigma^2_{(ellipse)})}{\sigma^2_{(circle)}}$$

referred to by Hart and Rudman (1997) as the reduction in variance. R^2 is the percentage of the variance from the circular model, which has been removed by the elliptical model. A value of 1.0 (100%) would indicate a perfect fit to an elliptical model whilst low values (~0.2 or 20%) indicate essentially isotropic behaviour. Hart and Rudman (1997) describe a least-squares elliptical fitting routine using Maple™, whilst an implementation using Fortran has been used here (Williamson, 1998). R^2 has been calculated for all data that conform to a single ellipse and only those data that generate a value greater than or equal to 70% have been considered for further processing. It was not possible to calculate a reduction in variance for data that conformed to a double-lobed ellipse.

5.3 PARAMETERS DERIVED FROM THE AZIMUTHAL DATA

5.3.1 Fracture orientation

Assuming the anisotropy is due to fracturing, the fracture orientation is obtained directly from the data. For single lobed ellipses, indicating only one primary fracture set, it is parallel to the minor axis of the fitted ellipse. For double lobed ellipses, the two orientations are taken from a visual inspection of the polar plot and are perpendicular to the azimuths of the local maxima. Orientation may change towards the cliff face and locally with structure. All quoted fracture azimuths are relative to local grid co-ordinates.

5.3.2 Quantitative measures of anisotropy

The coefficient of anisotropy, λ, as defined by

$$\lambda = \frac{\rho_{at}}{\rho_{al}}$$

where ρ_{at} is equivalent to the ellipse major axis and ρ_{al} to the minor axis. For doubled-lobed ellipses λ has been calculated as the local maximum value on the lobe divided by the minimum value recorded.

An alternative measure of anisotropy is given by the percentage variation about the average value of measurements plotted in the polar diagram (Nunn et al., 1983), i.e.

$$\pm 0.5\left[\frac{(\rho_{\max} - \rho_{\min})}{\rho_{average}}\right]100\%$$

However, this percentage variation is valid only for single-lobed ellipses and it has not therefore been calculated for double-lobed ellipses.

Variations in the quantitative measures of anisotropy between research sites may be related to fracture intensity or to factors such as fracture aperture and fracture porosity (Taylor and Fleming, 1988; Lane et al., 1995). Changes in λ or the percentage variation measured over time at the same locality may indicate seasonal cyclical variations or changes in fracture dilatancy or compression.

5.3.3 Temporal variations in the apparent resistivity measured

The apparent resistivity measured will vary with alterations within the rock mass (fracture dilatancy, moisture content etc.). Two apparent resistivity measures have been calculated. The first is the arithmetic average of the twelve measurements taken in each azimuthal set-up. The second is the root mean square (rms) differences between the twelve measurements taken in each azimuthal set-up and the values recorded during the initial visit in August/September 2001.

6 Field results

The main results from the two years of measurements from each of the five research sites are summarised in this section. Plots of representative data are given in the Appendix.

6.1 BEACHY HEAD

6.1.1 Tabulated parameters

	Site A a = 5 m					Site B a = 5 m					Site B a = 10 m				
Date	R^2	Az	λ	% aniso	Av ρ_a	R^2	Az	λ	% aniso	Av ρ_a	R^2	Az	λ	% aniso	Av ρ_a
Aug 01	85%	91°	2.24	±57.49%	248.56	95%	86°	2.48	±48.22%	240.92	90%	90°	2.95	±49.86%	272.67
Oct 01	95%	91.9°	1.73	±31.45%	235.03	97%	91.6°	1.74	±31.34%	230.73	93%	94.5°	2.51	±44.38%	256.27
Jan 02	81%	98.3°	1.53	±30.55%	262.2	97%	91.2°	2.01	±39.61%	260.59	93%	94.6°	2.61	±46.64%	286.95
Mar 02	87%	89°	1.4	±22.06%	227.84	96%	92.4°	1.67	±29.24%	225.56	95%	94.5°	2.11	±35.71%	262.63
Apr 02	85%	89.8°	1.83	±40.26%	260.98	94%	92°	2.30	±50.80%	254.31	91%	92.8°	2.85	±47.99%	291.05
Jul 02	85%	90°	2.19	±53.51%	265.0	95%	89°	2.58	±55.73%	254.43	89%	91°	3.13	±54.36%	290.12
Sep 02	84%	86.5°	2.48	±62.62%	272.75	93%	89.7°	3.13	±66.54%	259.65	89%	93.7°	3.32	±57.16%	292.99
Nov 02	95%	92.8°	1.99	±41.31%	284.6	97%	91.3°	2.24	±45.52%	273.14	90%	93.8°	3.29	±56.69%	297.70
Jan 03	91%	86.1°	1.67	±32.03%	233.27	96%	91.0°	1.94	±39.13%	221.36	94%	92.6°	2.38	±41.12%	266.39
Mar 03	93%	87.6°	1.68	±30.82%	243.1	96%	91.9°	1.88	±36.33%	235.0	94%	93.9°	2.40	±42.39%	277.36
May 03	86%	88.5°	2.13	±51.16%	275.51	93%	90.8°	2.51	±56.43%	263.67	90%	92.7°	3.09	±53.51%	305.69
July 03	83%	100.5°	2.21	±55.20%	271.61	92%	91.8°	2.54	±57.95%	256.13	91%	93.4°	3.12	±53.95%	298.60

	Site C a = 5 m					Site C a = 10 m					Site C a = 17 m				
Date	R^2	Az	λ	% aniso	Av ρ_a	R^2	Az	λ	% aniso	Av ρ_a	R^2	Az	λ	% aniso	Av ρ_a
Aug 01					173.63					197.31	95%	80.5°	1.49	±23.38%	214.56
Oct 01					168.09					193.54	89%	81.6°	1.24	±13.0%	204.73
Jan 02					189.86					210.4	93%	85.3°	1.32	±16.76%	220.0
Mar 02					171.26					201.47	94%	89.7°	1.31	±15.07%	215.74
Apr 02					185.9					210.15	94%	82.3°	1.44	±23.19%	223.26
Jul 02	74%				182.91	59%				209.66	94%	79.0°	1.45	±23.93%	220.62
Sep 02					180.18					208.43	96%	79.4°	1.44	±21.37%	221.53
Nov 02	66%				196.61	25%				212.29	94%	82.7°	1.40	±20.11%	214.67
Jan 03					160.63					197.62	95%	86.8°	1.30	±15.5%	215.80
Mar 03					173.47					205.69	94%	87.8°	1.34	±17.42%	220.15
May 03					190.3					217.3	95%	81.5°	1.46	±23.67%	228.42
July 03					181.84					216.75	96%	82.3°	1.47	±22.59%	228.74

	Control a = 5 m					Control a = 10 m					Control a = 17 m				
Date	R^2	Az	λ	% aniso	Av ρ_a	R^2	Az	λ	% aniso	Av ρ_a	Az_1	Az_2	λ_1	λ_2	Av ρ_a
Aug 01	51%	N/A	N/A	N/A	189.98	84%	185.8°	1.06	±3.61%	173.77	39.0°	151.5°	1.02	1.05	152.22
Oct 01	64%	N/A	N/A	N/A	175.91	34%	N/A	N/A	N/A	174.74	39.0°	154.0°	1.02	1.05	156.57
Jan 02	43%	N/A	N/A	N/A	198.79	86%	152.7°	1.05	±3.50%	180.78	39.0°	159.0°	1.03	1.10	155.96
Mar 02	79%	66°	1.03	±1.88%	171.44	19%	N/A	N/A	N/A	168.54	39.0°	144.0°	1.01	1.07	152.19
Apr 02	81%	20.5°	1.05	±2.67%	190.61	25%	N/A	N/A	N/A	176.43	39.0°	144.0°	1.01	1.07	153.07
Jul 02	93%	127°	1.14	±6.94%	189.36	88%	140°	1.13	±6.66%	182.01	-	159.0°	-	1.20	158.59
Sep 02	98%	135°	1.15	±7.16%	194.77	92%	149°	1.15	±7.92%	180.82	-	152.0°	-	1.22	157.47
Nov 02	84%	132.5°	1.12	±6.70%	200.17	87%	142.9°	1.13	±8.38%	189.49	-	159.0°	-	1.20	164.84
Jan 03	91%	143.4°	1.14	±7.95%	148.47	91%	152.8°	1.14	±8.88%	152.11	-	159.0°	-	1.18	143.99
Mar 03	96%	150.1°	1.11	±5.86%	173.83	95%	150.1°	1.14	±7.56%	174.46	-	144.0°	-	1.17	154.8
May 03	90%	142.4°	1.18	±10.04%	195.03	94%	150.8°	1.15	±8.39%	185.91	-	144.0°	-	1.20	159.24
July 03	98%	142.3°	1.20	±10.63%	194.27	96%	149.3°	1.17	±8.90%	188.04	-	144.0°	-	1.24	162.42

Key

$R^{2\,=}$ Reduction in variance

% aniso = Percentage anisotropy

Az = Azimuth of fracture strike

Av ρ_a = Average apparent resistivity (Ω.m)

λ = Coefficient of anisotropy

Note: The strike azimuth is relative to BNG grid north, but is based on a magnetic north compass bearing and an assumed magnetic declination of -6°. Site C 'a' = 5 & 10 m did not give satisfactory ellipses for estimating azimuthal parameters. At the Control Site for the spacing of 'a' = 17 m, where a double-lobed ellipse was measured, λ was calculated as the major axis of the ellipse lobe divided by the minimum value recorded. After July 2002 the data here conformed to a single peaked ellipse, but for continuity λ was still calculated as the major axis of the ellipse divided by the minimum value recorded. However, R^2 values were calculated and ranged between 89 to 97%.

6.1.2 Graphical plots of parameters

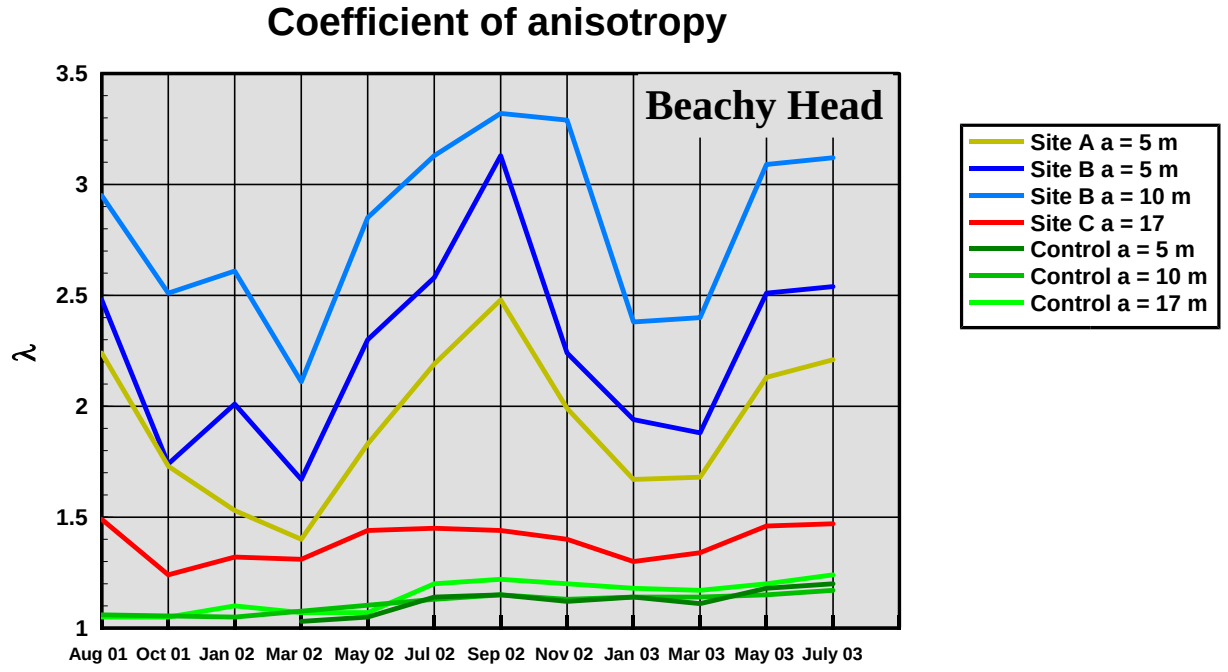

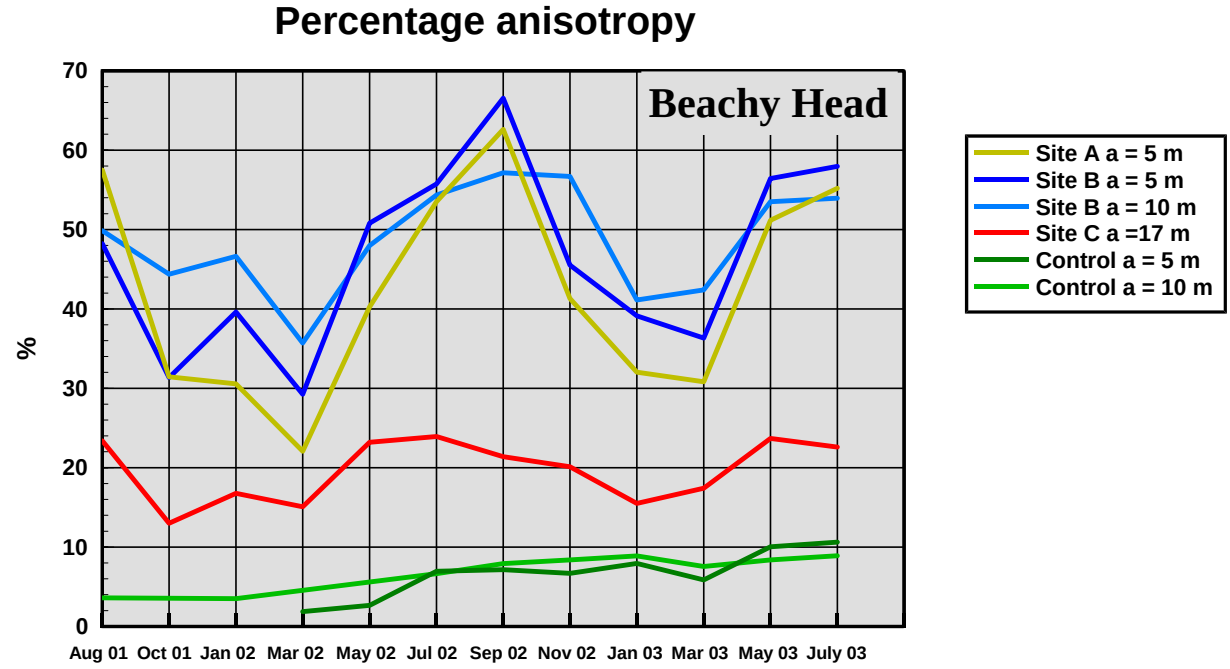

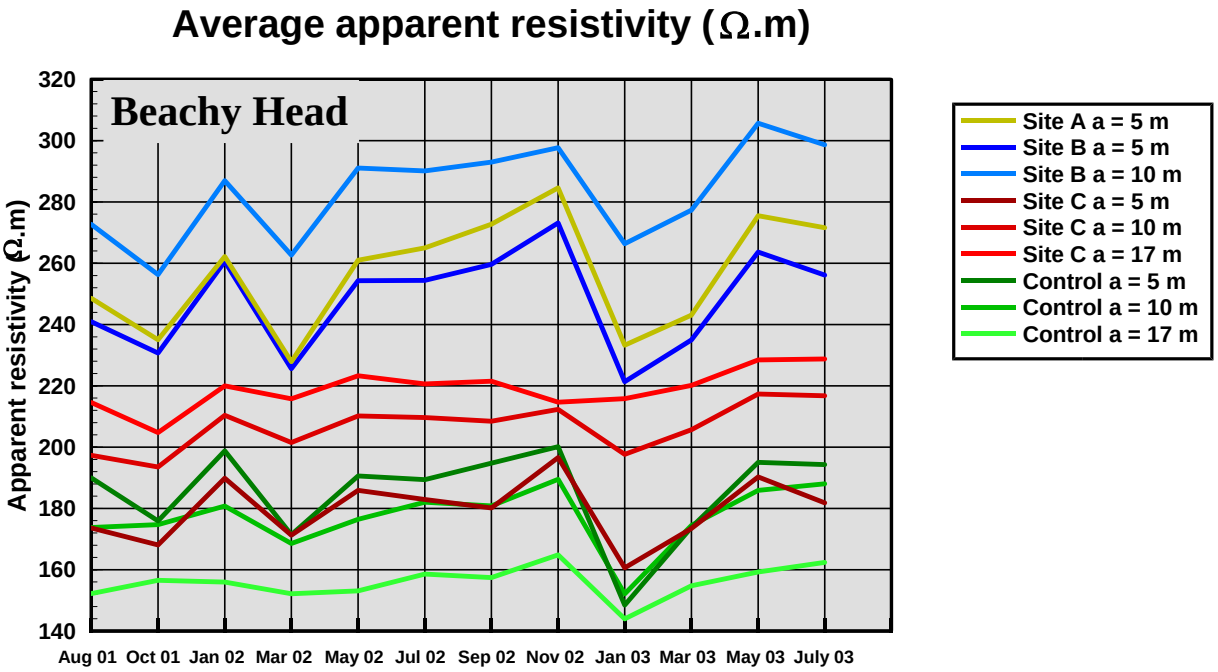

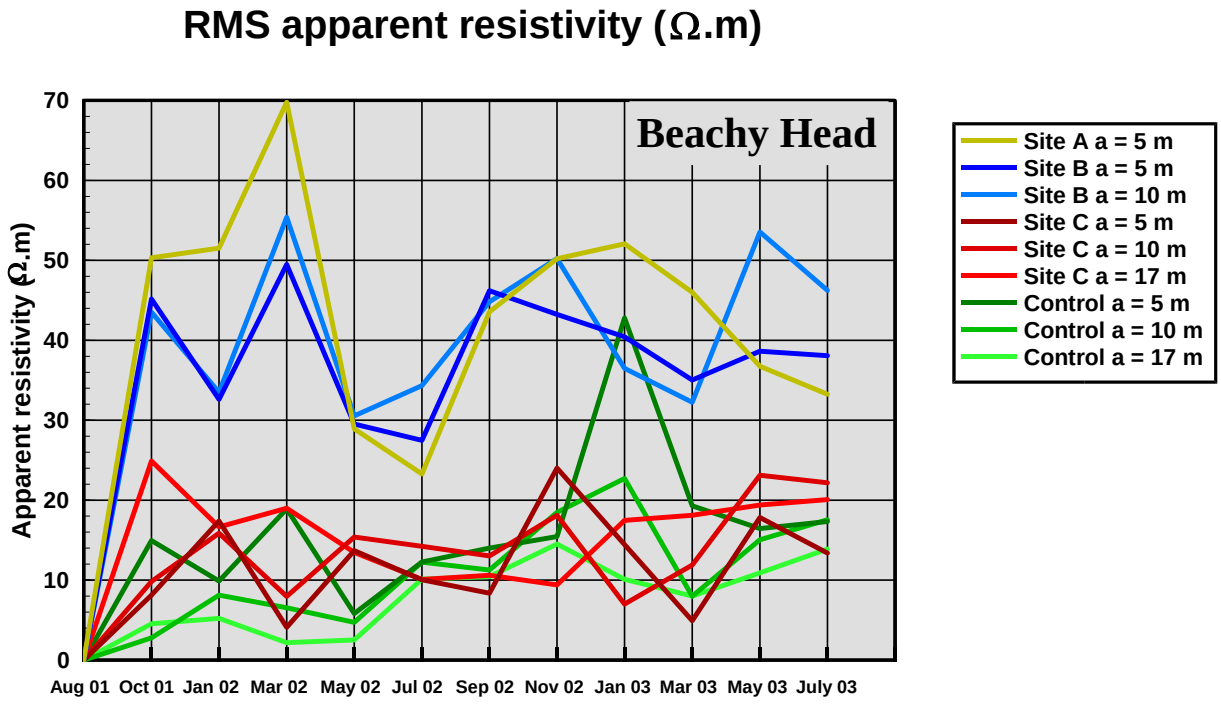

6.1.3 Results summary

Assuming the anisotropy can be related to fracturing, the orientations of the primary fracture sets derived from the azimuthal apparent resistivity data are as follows

A, a = 5 m	B, a = 5 m	B, a = 10 m	C, a = 17 m	Control a = 17 m
91°	91°	93°	83°	151°

This indicates a fracture set parallel to the cliff, near the cliff edge and a tectonic fracture set at the Control Site. The estimate of the tectonic fracture set orientation agrees with recent mapping (see above).

The quantitative measures of anisotropy both display a strong seasonal variation, especially towards the cliff edge. Values peak in the summer (July – September) with minimum values in the winter (January – March). A similar pattern is seen at the Control Site although the magnitudes of the anisotropy measures are much less and there is a gradual increase over the monitoring period.

The average resistivities show very constant values with a small peak in November 2002 and minimum values between January - March 2003. There is a gradual increase in resistivity towards the cliff edge, probably reflecting the increased drainage. The greatest variations in the rms apparent resistivites occur towards the cliff edge and they display a seasonal variation similar to that observed in λ and the percentage anisotropy.

6.2 BIRLING GAP

6.2.1 Tabulated parameters

	Site A a = 5 m					Site B a = 5 m					Site B a = 10 m				
Date	R^2	Az	λ	% aniso	Av ρ_a	R^2	Az	λ	% aniso	Av ρ_a	R^2	Az	λ	% aniso	Av ρ_a
Aug 01	93%	111.8°	2.46	±63.70%	98.38	96%	111.7°	1.55	±22.74%	99.09	97%	114.0°	2.07	±38.16%	112.28
Oct 01	94%	113.3°	2.37	±58.85%	101.87	90%	110.9°	1.41	±19.81%	103.4	98%	112.8°	1.93	±33.07%	111.7
Jan 02	95%	110.0°	2.45	±59.99%	120.90	92%	109.8°	1.39	±18.59%	117.2	98%	111.0°	2.00	±36.48%	122.92
Mar 02	92%	112.4°	2.21	±53.97%	115.98	93%	109.1°	1.44	±19.55%	118.12	98%	113.6°	1.91	±32.88%	123.36
Apr 02	-	-	-	-	-	92%	112.2°	1.60	±26.96%	117.54	-	-	1.75	-	-
Jul 02	90%	106.4°	1.42	±18.14%	107.52	86%	104.9°	1.23	±13.55%	107.2	85%	122.0°	1.67	±33.94%	114.77
Sep 02	93%	106.6°	1.47	±19.39%	108.39	77%	99.2°	1.24	±16.02%	106.66	84%	122.5°	1.63	±32.56%	113.87
Nov 02	91%	108.8°	1.50	±19.18%	121.06	82%	117.2°	1.19	±10.89%	120.84	95%	123.2°	1.67	±30.24%	120.69
Jan 03	91%	110.6°	1.47	±19.33%	117.45	71%	117.8°	1.16	±11.55%	109.45	90%	125.7°	1.64	±31.08%	121.25
Mar 03	88%	113.0°	1.48	±17.74%	119.64	71%	125.9°	1.13	±8.56%	113.96	91%	127.4°	1.65	±30.31%	123.8
May 03	89%	112.1°	1.63	±21.67%	117.45	84%	121.2°	1.22	±12.48%	113.41	88%	128.0°	1.84	±37.99%	124.64
July 03	89%	112.7°	1.60	±20.59%	113.15	83%	119.6°	1.21	±11.97%	110.48	89%	127.8°	1.81	±36.74%	121.88

	Site C a = 5 m					Site C a = 10 m					Site C a = 20 (or 17) m				
Date	R^2	Az	λ	% aniso	Av ρ_a	R^2	Az	λ	% aniso	Av ρ_a	Az_1	Az_2	λ_1	λ_2	Av ρ_a
Aug 01	78%	70.6°	1.11	±8.42%	96.52	97%	81.0°	1.28	±12.09%	93.66	84.0°	144.0°	1.53	1.43	89.58
Oct 01	67%	N/A	N/A	N/A	103.65	97%	82.6°	1.29	±12.44%	95.70	84.0°	144.0°	1.48	1.44	89.28
Jan 02	9%	N/A	N/A	N/A	113.02	97%	84.9°	1.27	±12.04%	100.51	84.0°	144.0°	1.45	1.39	91.56
Mar 02	50%	N/A	N/A	N/A	119.67	96%	92.5°	1.23	±11.21%	102.88	84.0°	144.0°	1.47	1.45	93.28
Apr 02	42%	N/A	N/A	N/A	113.49	96%	95.1°	1.26	±12.26%	101.61	84.0°	144.0°	N/A	1.26	90.05
Jul 02	55%	N/A	N/A	N/A	113.27	94%	99.3°	1.25	±12.23%	102.27	84.0°	144.0°	1.35	1.41	95.48
Sep 02	54%	N/A	N/A	N/A	111.14	96%	94.4°	1.28	±13.86%	101.03	84.0°	144.0°	1.38	1.40	94.28
Nov 02	49%	N/A	N/A	N/A	128.96	97%	90.6°	1.26	±12.44%	106.55	84.0°	144.0°	1.33	1.40	97.22
Jan 03	61%	N/A	N/A	N/A	113.05	95%	97.6°	1.27	±13.52%	104.29	84.0°	144.0°	1.30	1.42	98.57
Mar 03	-	N/A	N/A	N/A	120.76	93%	98.5°	1.25	±13.77%	107.22	84.0°	144.0°	1.29	1.44	99.74
May 03	-	N/A	N/A	N/A	120.67	94%	100.7°	1.27	±13.44%	107.26	84.0°	144.0°	1.31	1.50	99.43
July 03	-	N/A	N/A	N/A	118.29	95%	100.2°	1.28	±13.64%	106.82	84.0°	144.0°	1.30	1.48	99.43

	Control a = 5 m					Control a = 10 m					Control a = 20 m				
Date	R^2	Az	λ	% aniso	Av ρ_a	R^2	Az	λ	% aniso	Av ρ_a	R^2	Az	λ	% aniso	Av ρ_a
Aug 01	99%	67.6°	1.30	±12.99%	134.21	98%	69.2°	1.80	±30.09%	108.53	98%	72.2°	2.19	±43.12%	78.85
Oct 01	97%	69.4°	1.21	±9.21%	131.08	98%	71.9°	1.60	±24.46%	109.83	99%	74.2°	2.01	±36.43%	80.68
Jan 02	96%	64.6°	1.27	±12.12%	143.77	98%	69.5°	1.69	±27.18%	112.07	98%	73.1°	2.12	±39.98%	79.94
Mar 02	86%	69.2°	1.16	±9.21%	130.99	98%	71.5°	1.51	±21.52%	108.91	98%	73.7°	1.96	±35.59%	79.72
Apr 02	87%	66.7°	1.21	±11.61%	140.91	98%	70.7°	1.68	±24.59%	112.1	98%	73.7°	2.06	±37.92%	79.19
Jul 02	97%	72.8°	1.22	±10.51%	137.83	98%	73.4°	1.63	±23.03%	114.1	98%	73.7°	2.04	±35.72%	81.38

Sep 02	94%	69.1°	1.25	±12.45%	137.81	99%	70.8°	1.69	±25.24%	113.88	98%	73.8°	2.1	±38.93%	81.83
Nov 02	93%	67.1°	1.18	±8.62%	136.89	99%	71.2°	1.54	±21.93%	119.10	98%	73.2°	1.98	±36.02%	85.16
Jan 03	89%	62.7°	1.21	±10.51%	112.03	98%	69.4°	1.51	±19.84%	103.55	99%	71.5°	1.83	±31.62%	80.72
Mar 03	96%	66.3°	1.20	±8.73%	129.03	98%	70.6°	1.53	±20.75%	110.36	98%	73.0°	1.87	±33.57%	80.52
May 03	97%	69.5°	1.25	±11.40%	138.81	97%	73.6°	1.65	±23.98%	116.06	98%	73.8°	2.01	±36.20%	81.77
July 03	98%	70.5°	1.28	±12.51%	137.14	98%	72.0°	1.68	±24.50%	117.53	98%	74.4°	2.04	±37.05%	83.66

Key

R^{2} = Reduction in variance

Az = Azimuth of fracture strike

λ = Coefficient of anisotropy

% aniso = Percentage anisotropy

Av ρ_a = Average apparent resistivity (Ω.m)

Note: The strike azimuth is relative to BNG grid north, but is based on a magnetic north compass bearing and an assumed magnetic declination of -6°.

The λ values for Site C, 'a' = 20/17 m are calculated along two azimuths corresponding to ellipse peaks at 84° and 144° and are calculated as lobe maximum values divided by the minimum value recorded.

The cliff fall between the beginning of March and the end of April 2002 removed a small section of the upper cliff directly at the measurement site. An incomplete data set was collected in April 2002.

6.2.2 Graphical plots of parameters

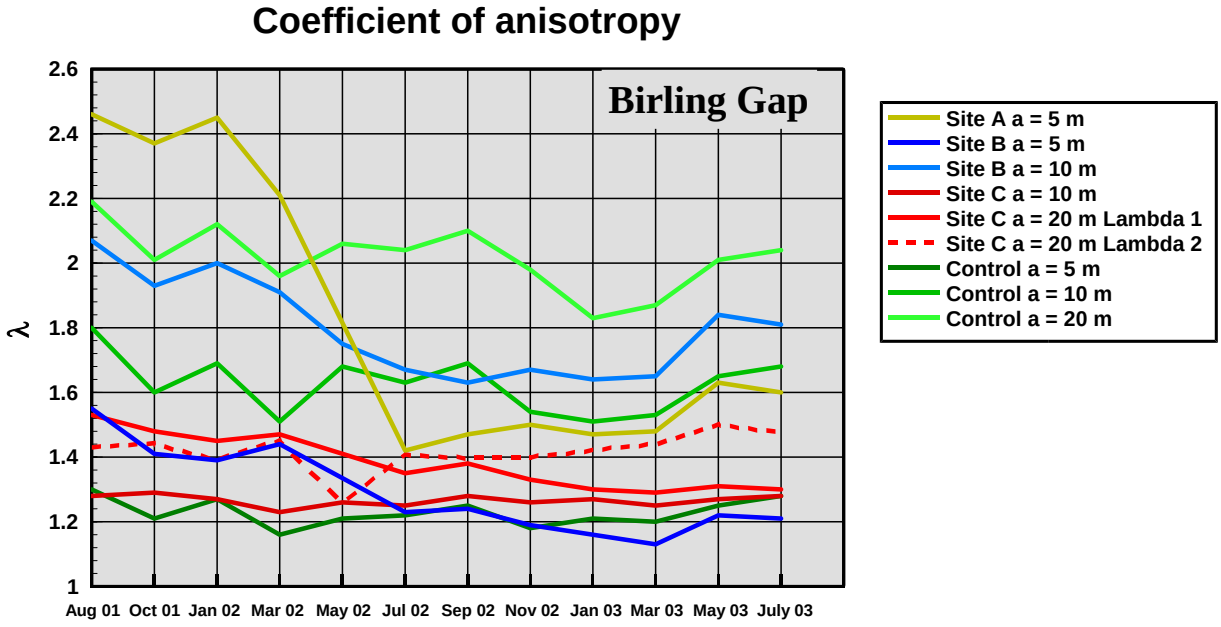

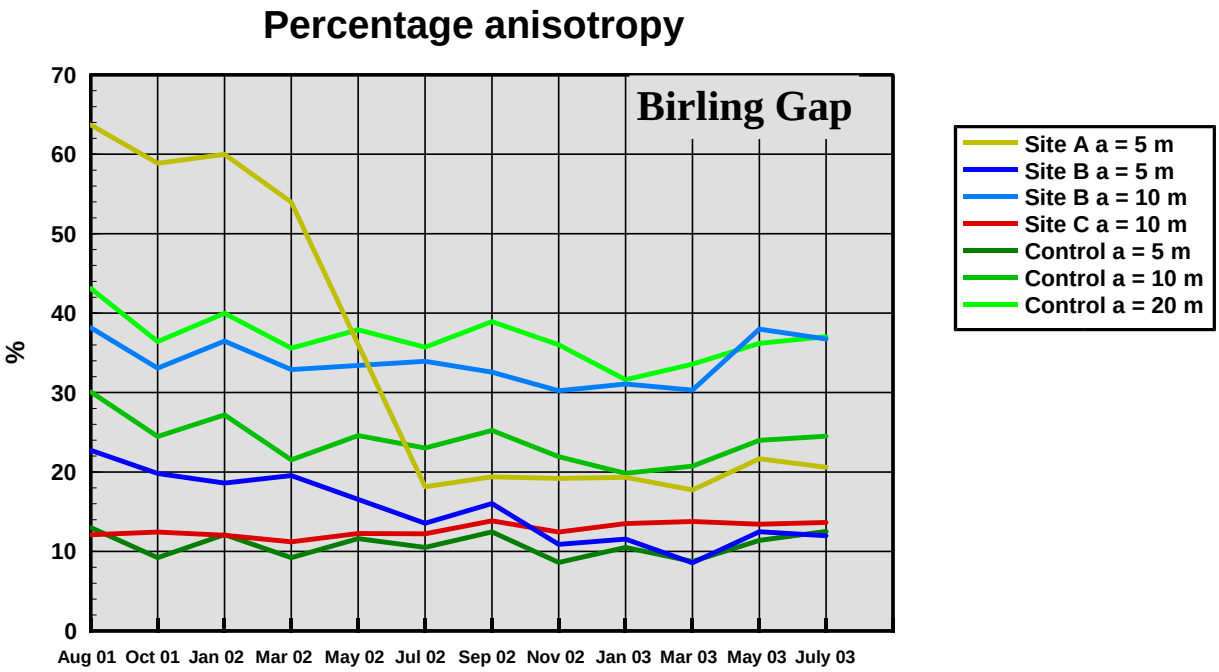
Percentage anisotropy
Birling Gap
%
70
60
50
40
30
20
10
0
Aug 01 Oct 01 Jan 02 Mar 02 May 02 Jul 02 Sep 02 Nov 02 Jan 03 Mar 03 May 03 July 03
Site A a = 5 m
Site B a = 5 m
Site B a = 10 m
Site C a = 10 m
Control a = 5 m
Control a = 10 m
Control a = 20 m

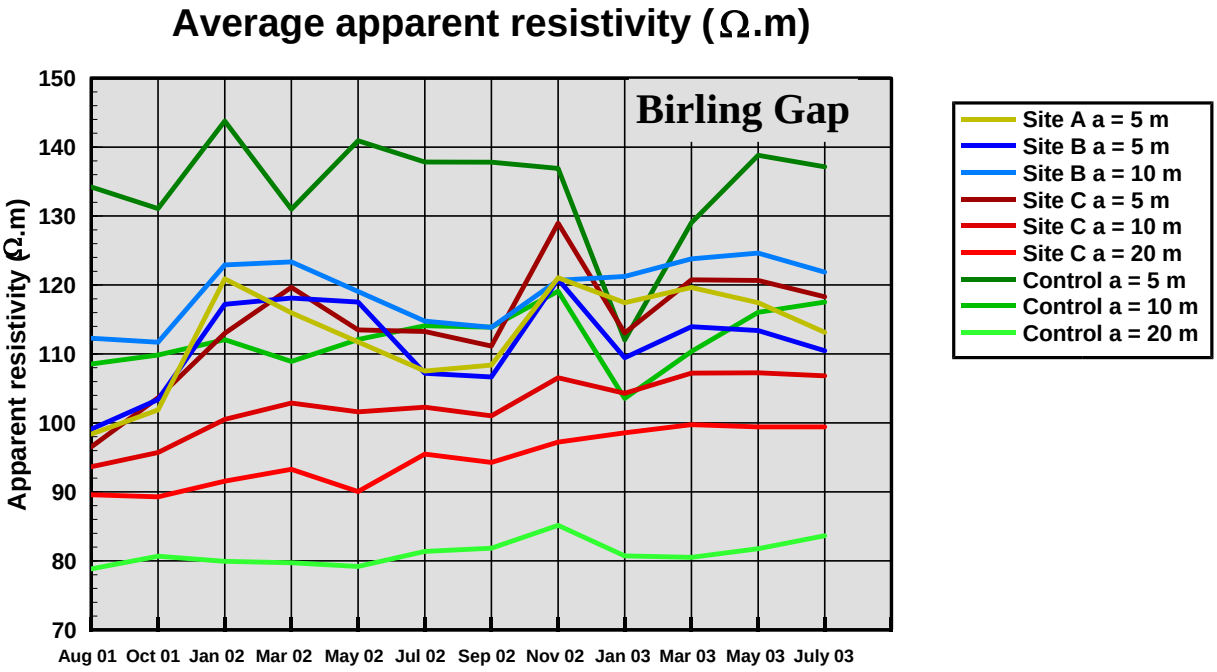
Average apparent resistivity (Ω.m)
Birling Gap
Apparent resistivity (Ω.m)
150
140
130
120
110
100
90
80
70
Aug 01 Oct 01 Jan 02 Mar 02 May 02 Jul 02 Sep 02 Nov 02 Jan 03 Mar 03 May 03 July 03
Site A a = 5 m
Site B a = 5 m
Site B a = 10 m
Site C a = 5 m
Site C a = 10 m
Site C a = 20 m
Control a = 5 m
Control a = 10 m
Control a = 20 m

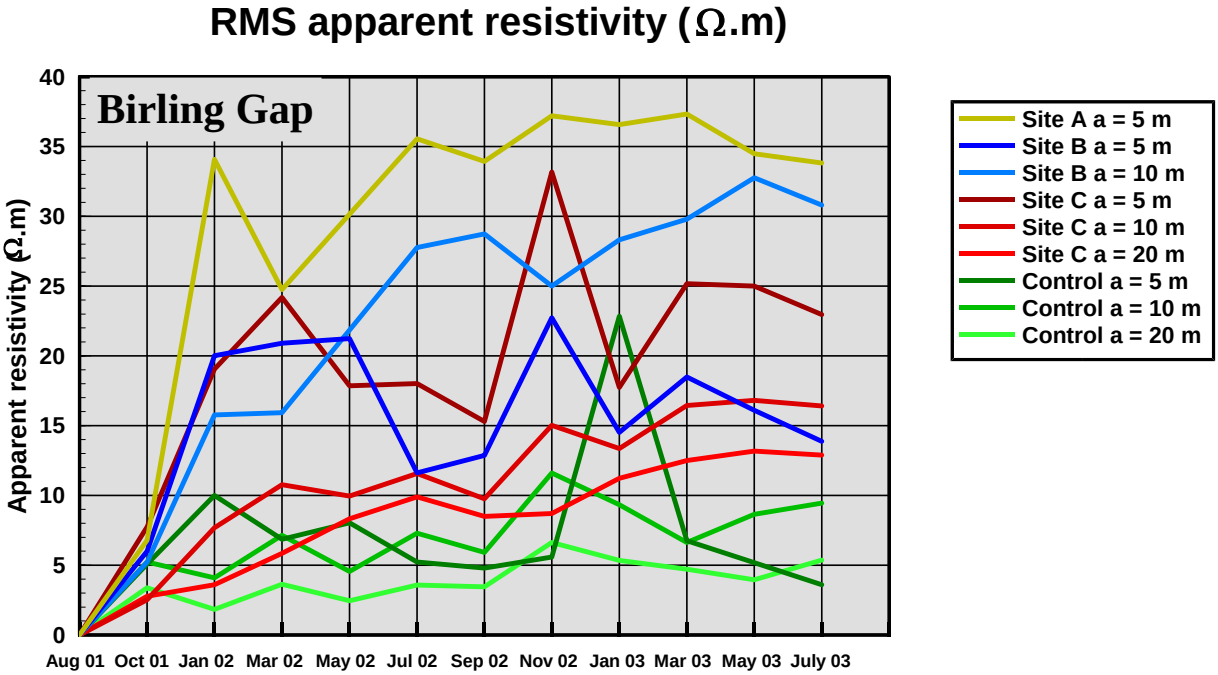

6.2.3 Results summary

Again, if the anisotropy can be related to fracturing, the orientations of the primary fracture sets derived from the azimuthal apparent resistivity data are as follows.

A, a = 5 m	B, a = 5 m	B, a = 10 m	C, a = 10 m	C, a = 17/20 m	Control a = 5 m	Control a = 10 m	Control a = 20 m
111°	113°	121°	93°	84° & 144°	68°	71°	73°

This indicates a fracture set parallel to the cliff, near the cliff edge, although the orientations derived from Site C a = 17/20 m do not fit this pattern. The estimated tectonic fracture orientation at the Control Site also agrees with recent mapping (see above).

The plots of the quantitative measures of anisotropy are dominated by the reduction in values for Site A after the cliff fall in 2002. The coefficient of anisotropy also shows similar changes for the Site B measurement, but this is not shown by the percentage anisotropy. There are no associated variations at the Control Site suggesting that the changes are related to the cliff fall. There is no indication of the January 2003 cliff fall where the ground lost was outside of the actual measurement. Seasonal variations are much less than at Beachy Head, but the same cycle is evident particularly in the control data. The quantitative measures of anisotropy from the Control Site at Birling Gap are much greater than their equivalents at Beachy Head. This is thought to be associated with the style of fracturing.

The temporal variations associated with the average resistivities are similar to Beachy Head with a small peak in November 2002 and minimum values around January 2003. Unlike Beachy Head there is little evidence for a resistivity gradient toward the cliff edge. There appears to be little pattern in the rms apparent resistivities.

6.3 MESNIL-VAL

6.3.1 Tabulated parameters

	Site A a = 5 m					Site B a = 5 m					Site B a = 10 m				
Date	R^2	Az	λ	% aniso	Av ρ_a	R^2	Az	λ	% aniso	Av ρ_a	R^2	Az	λ	% aniso	Av ρ_a
Aug 01	83%	54.5°	2.52	±75.04%	288.2	88%	42.6°	1.29	±14.00%	265.61	92%	55.0°	1.83	±30.66%	245.14
Oct 01	91%	54.6°	2.01	±50.36%	270.75	96%	38.8°	1.18	±9.82%	243.52	92%	56.8°	1.61	±25.46%	246.02
Jan 02	94%	57.8°	1.77	±36.42%	279.78	90%	41.9°	1.15	±7.87%	269.59	95%	56.6°	1.49	±19.6%	244.95
Mar 02	89%	60°	1.61	±30.57%	224.29	68%	-	-	-	228.82	66%	-	-	-	210.03
Apr 02	90%	62.3°	2.33	±55.37%	282.44	96%	29.9°	1.21	±10.57%	284.86	90%	60.4°	1.59	±26.59%	237.71
Jul 02	89%	58.6°	1.96	±45.02%	269.83	91%	32.8°	1.33	±17.79%	268.94	86%	61.0°	1.46	±21.47%	242.87
Sep 02	83%	60°	2.66	±72.70%	313.25	90%	24.5°	1.21	±10.75%	325.01	84%	61.2°	1.56	±27.43%	253.84
Nov 02	84%	57.2°	1.56	±29.32%	244.43	94%	22.3°	1.13	±6.2%	241.8	76%	53.3°	1.26	±14.73%	241.26
Jan 03	90%	57.8°	1.72	±36.51%	260.37	92%	33.1°	1.11	±5.99%	249.98	90%	57.4°	1.39	±17.86%	247.19
Mar 03	85%	63.4°	1.80	±38.51%	273.84	80%	46.2°	1.07	±3.61%	277.23	88%	62.2°	1.46	±20.21%	254.50
May 03	83%	59.6°	2.02	±51.53%	292.02	98%	40.1°	1.21	±9.52%	306.26	91%	60.9°	1.62	±27.08%	263.50
July 03	81%	59.7°	2.05	±54.47%	282.29	93%	39.1°	1.20	±11.10%	296.3	91%	60.9°	1.57	±26.32%	264.46

	Site C a = 5 m					Site C a = 10 m					Site C a = 20 m				
Date	R^2	Az	λ	% aniso	Av ρ_a	R^2	Az	λ	% aniso	Av ρ_a	R^2	Az	λ	% aniso	Av ρ_a
Aug 01					229.48	97%	56.4°	1.26	±11.79%	207.03	97%	60.1°	1.74	±29.16%	179.38
Oct 01					212.56	87%	56.5°	1.23	±14.34%	208.34	95%	58.3°	1.69	±29.35%	182.81
Jan 02					262.61	97%	60.9°	1.31	±13.82%	229.55	94%	60.3°	1.67	±26.91%	176.3
Mar 02					221.53	93%	66.6°	1.19	±9.55%	216.22	78%	64.0°	1.47	±25.51%	163.29
Apr 02					273.12	95%	63.9°	1.31	±14.81%	230.43	95%	62.5°	1.71	±26.82%	171.53
Jul 02					248.47	91%	48.4°	1.14	±7.89%	243.87	87%	62.1°	1.51	±23.98%	178.32
Sep 02					302.89	96%	63.1°	1.32	±15.55%	251.05	98%	63.7°	1.78	±30.82%	184.03
Nov 02					227.92	91%	63.1°	1.14	±7.46%	240.53	79%	61.7°	1.44	±23.3%	188.14
Jan 03					234.94	97%	59.5°	1.32	±14.76%	226.9	94%	60.7°	1.67	±26.83%	188.69
Mar 03					267.70	96%	61.8°	1.31	±13.76%	242.91	94%	63.5°	1.73	±28.93%	187.95
May 03					-	96%	63.4°	1.34	±15.85%	253.95	95%	62.8°	1.79	±30.28%	189.25
July 03					279.08	90%	62.5°	1.18	±9.12%	257.14	94%	62.9°	1.65	±25.60%	193.30

	Control a = 5 m					Control a = 10 m					Control a = 20 m				
Date	R^2	Az	λ	% aniso	Av ρ_a	Az_1	Az_2	λ_1	λ_2	Av ρ_a	Az_1	Az_2	λ_1	λ_2	Av ρ_a
Aug 01	85%	6°	1.34	±17.21%	154.23	9°	129°	1.52	1.29	135.27	24°	114°	2.25	2.20	103.74
Oct 01	96%	7.3°	1.28	±12.83%	154.68	9°	129°	1.42	1.22	142.07	16.5°	114°	1.96	1.81	109.32
Jan 02	96%	7.1°	1.25	±11.16%	192.26	9°	129°	1.39	1.17	158.95	16.5°	114°	1.78	1.78	112.77
Mar 02	96%	6.6°	1.18	±8.54%	175.75	9°	129°	1.35	1.22	153.78	16.5°	122°	1.65	1.62	112.82
Apr 02	96%	1.5°	1.45	±20.52%	192.09	9°	129°	1.56	1.39	153.06	9°	121.5°	2.39	2.34	106.22
Jul 02	85%	15.5°	1.24	±13.68%	199.0	9°	129°	1.42	1.22	169.96	9°	114°	1.89	1.82	116.94
Sep 02	98%	4.2°	1.44	±18.18%	197.65	9°	129°	1.57	1.37	159.67	16.5°	114°	2.29	2.29	109.19
Nov 02	97%	11.6°	1.44	±11.59%	171.17	9°	129°	1.37	1.17	164.63	24°	114°	1.89	1.76	121.80
Jan 03	95%	5.2°	1.25	±11.72%	176.11	9°	129°	1.34	1.18	160.81	16.5°	121.5°	1.47	1.44	121.80
Mar 03	96%	2.6°	1.28	±12.50%	193.02	9°	129°	1.41	1.26	164.45	16.5°	114°	1.84	1.79	116.63
May 03	98%	0.9°	1.35	±13.51%	200.46	9°	129°	1.48	1.34	166.06	9°	121.5°	2.11	2.07	115.12
July 03	95%	14.9°	1.40	±19.33%	190.03	9°	129°	1.54	1.24	170.22	16.5°	114°	2.0	1.87	120.63

Key

R^2 = Reduction in variance

% aniso = Percentage anisotropy

Az = Azimuth of fracture strike

Av ρ_a = Average apparent resistivity (Ω.m)

λ = Coefficient of anisotropy

Note: The strike azimuth is relative to IGN grid north, and is based on a deviation of –21° between the grid and azimuthal array set-up.

Site C a = 5 m did not generate satisfactory ellipses for estimating azimuthal parameters. For the spacings of a = 10 and 20 m where a double ellipse was measured λ was calculated as the major axis of the ellipse lobe divided by the minimum value recorded.

6.3.2 Graphical plots of parameters

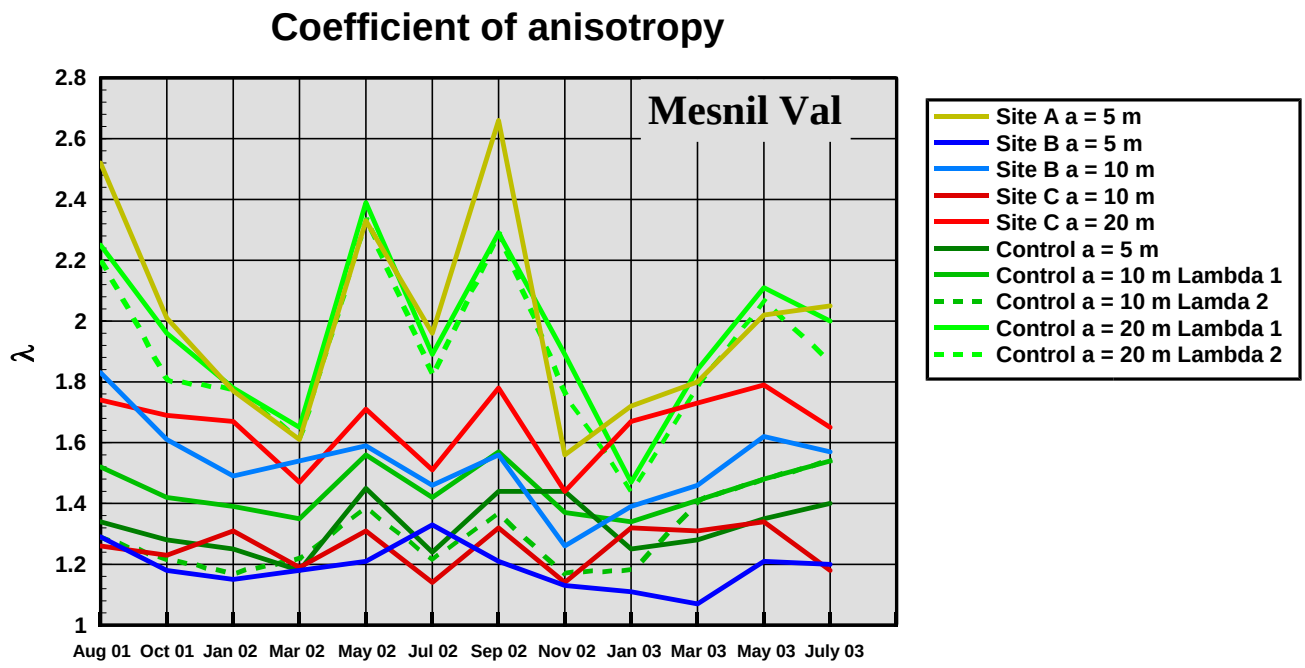

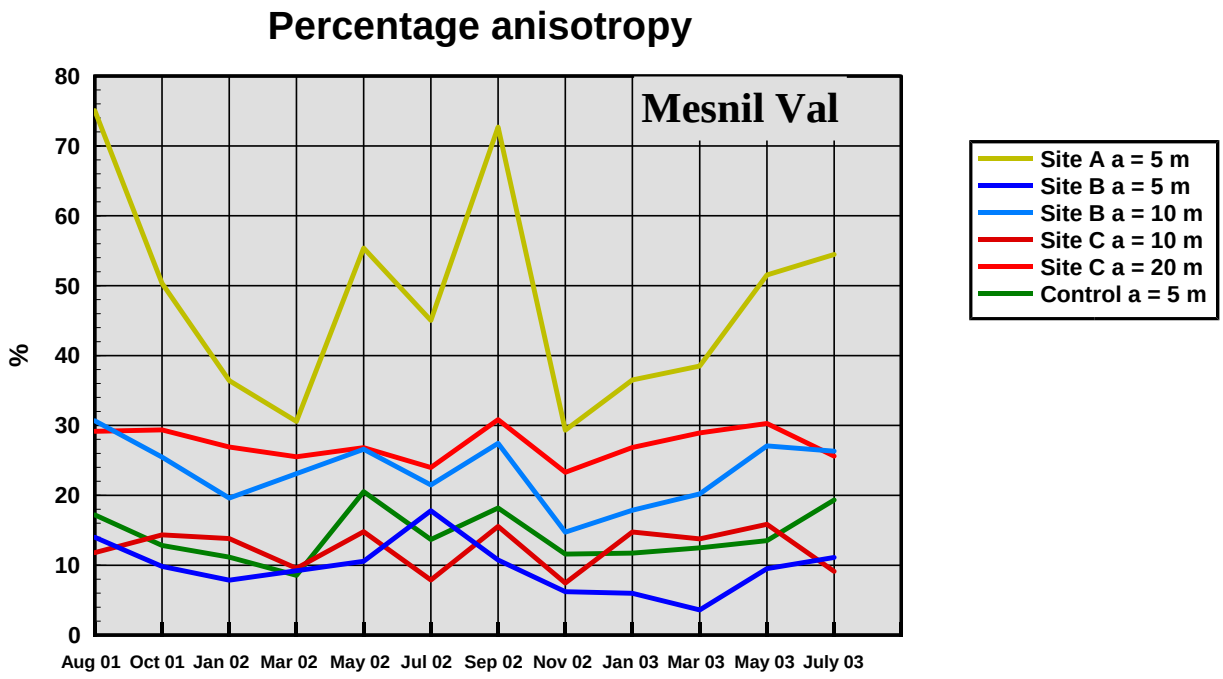

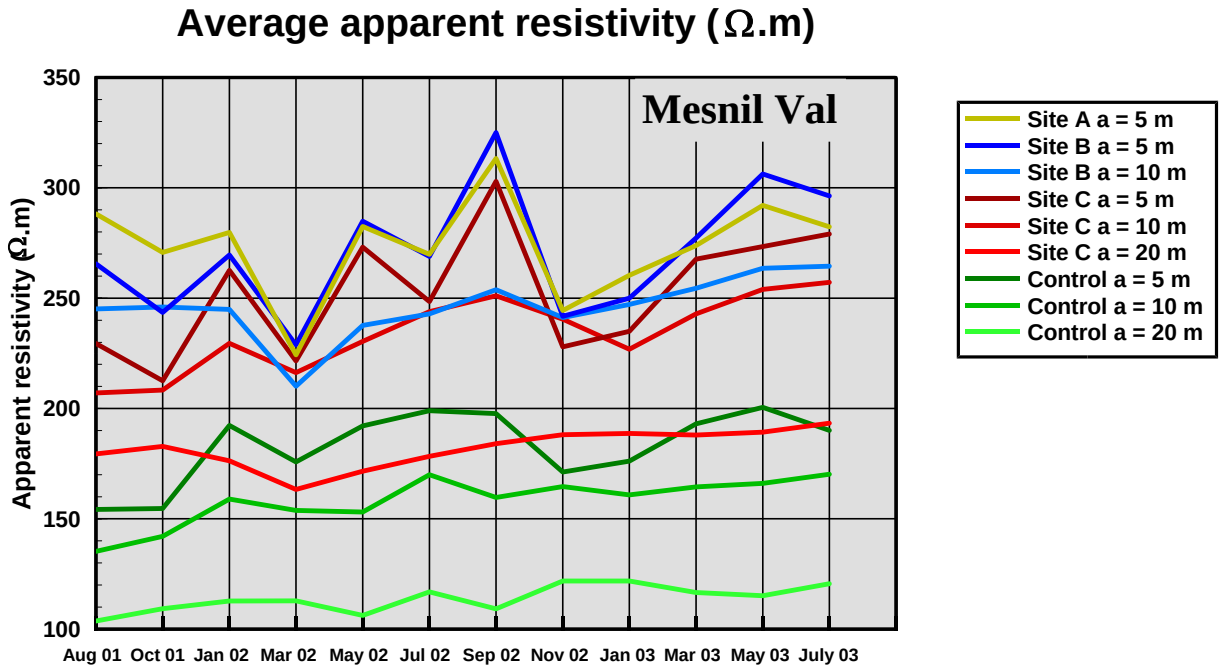

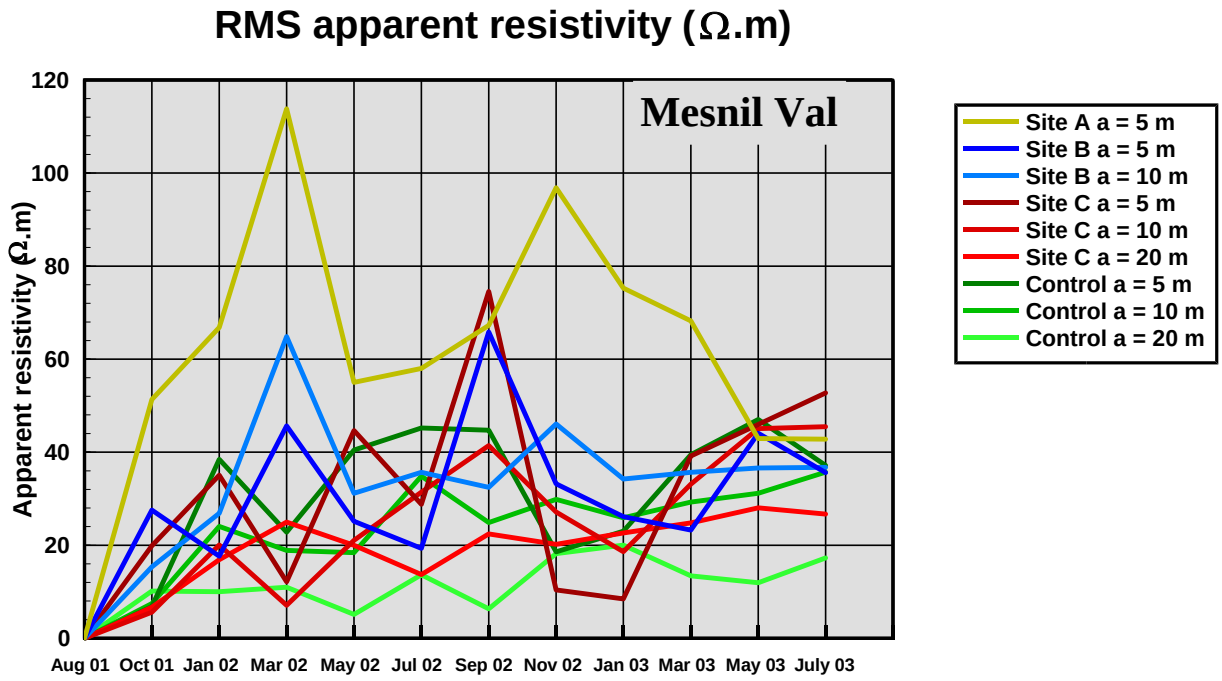

6.3.3 Results summary

If the anisotropy arises from fracturing, the interpreted orientations of the primary fracture sets are as follows.

A, a = 5 m	B, a = 5 m	B, a = 10 m	C, a = 10 m	C, a = 20 m	Control a = 5 m	Control a = 10 m	Control a = 20 m
59°	36°	59°	61°	62°	7°	9° & 129°	16° & 117°

This indicates a fracture set sub-parallel to the cliff face, near the cliff edge. The fracture orientations at the Control Site are in broad agreement with the mapped tectonic fracture azimuths (see above).

The quantitative measures of anisotropy display a strong seasonal variation. Values peak in the summer (May – September) with minimum values in the winter (November – March). The coefficient of anisotropy for the Control site 'a' = 20 m, shows the same magnitudes and pattern of variation as Site A. The cliff fall of June 23rd 2002 is not apparent in the data.

The average apparent resistivities display a gradual increase over the monitoring period, upon which is superimposed a seasonal variation. This results in higher values in the summer and lower values in the winter. The seasonal variations are more pronounced towards the cliff edge and there is an increase in resistivity towards the cliff. The rms apparent resistivities display some random variations, but a seasonal variation is also evident.

6.4 JÆTTEBRINK

6.4.1 Tabulated parameters

	Site A a = 5 m					Site B a = 5 m					Site B a = 10 m				
Date	R^2	Az	λ	% aniso	Av ρ_a	R^2	Az	λ	% aniso	Av ρ_a	R^2	Az	λ	% aniso	Av ρ_a
Sep 01	89%	135.0°	1.24	±12.35%	334.62	96%	167.4°	1.25	±10.71%	335.12	93%	171.8°	1.38	±17.86%	310.9
Nov 01	92%	117.2°	1.38	±17.74%	358.21	93%	147.9°	1.17	±6.90%	359.42	88%	167.6°	1.28	±15.70%	322.32
Jan 02	90%	122.8°	1.45	±20.28%	374.87	88%	157.4°	1.18	±10.93%	374.31	89%	165.2°	1.31	±15.03%	330.64
Mar 02	98%	124.9°	1.52	±20.63%	341.62	95%	155.2°	1.19	±9.10%	345.10	93%	164.1°	1.32	±16.69%	315.66
Apr 02	92%	125.9°	1.40	±16.06%	352.87	97%	159.6°	1.16	±7.95%	356.89	93%	168.2°	1.33	±16.91%	322.13
Jul 02	89%	130.4°	1.32	±13.69%	321.0	94%	155.4°	1.21	±9.89%	321.61	92%	165.1°	1.35	±17.60%	308.11
Aug 02	69%	N/A	N/A	N/A	312.24	95%	154.6°	1.20	±8.71%	311.04	92%	166.4°	1.32	±16.78%	299.71
Nov 02	94%	123.1°	1.47	±21.79%	362.98	96%	154.3°	1.16	±7.48%	360.07	92%	164.1°	1.29	±14.4%	321.79
Jan 03	97%	115.4°	1.52	±22.36%	398.0	93%	152.8°	1.19	±8.89%	391.84	90%	163.6°	1.26	±11.11%	338.85
Mar 03	94%	127.8°	1.44	±20.24%	418.89	94%	152.3°	1.17	±8.58%	409.58	94%	165.5°	1.34	±16.34%	348.53
May 03	92%	126.3°	1.42	±19.57%	387.38	95%	152.7°	1.19	±10.22%	384.26	94%	167.1°	1.36	±18.01%	344.19
July 03	88%	125.5°	1.28	±12.75%	336.43	97%	153.6°	1.17	±8.04%	331.81	91%	164.1°	1.30	±14.47%	316.69

	Site C a = 5 m					Site C a = 10 m					Site C a = 20 m				
Date	R^2	Az	λ	% aniso	Av ρ_a	R^2	Az	λ	% aniso	Av ρ_a	Az_1	Az_2	λ_1	λ_2	Av ρ_a
Aug 01	50%	N/A	N/A	N/A	312.94	54%	N/A	N/A	N/A	316.28	173°	128°	1.38	1.22	232.77
Oct 01	76%	79.7°	1.23	±13.95%	343.81	57%	N/A	N/A	N/A	326.51	173°	128°	1.34	1.23	233.05
Jan 02	88%	75.0°	1.26	±12.91%	361.58	44%	N/A	N/A	N/A	333.79	173°	128°	1.30	1.25	233.28
Mar 02	92%	77.3°	1.18	±7.99%	335.18	5%	N/A	N/A	N/A	318.84	173°	128°	1.33	1.22	228.55
Apr 02	87%	72.5°	1.18	±10.50%	347.64	40%	N/A	N/A	N/A	328.14	173°	128°	1.34	1.22	230.71
Jul 02	83%	74.3°	1.26	±14.68%	319.74	61%	N/A	N/A	N/A	315.21	173°	128°	1.30	1.21	230.73
Sep 02	92%	73.8°	1.29	±14.27%	299.36	74%	85.0°	1.11	±5.73%	306.0	173°	128°	1.21	1.20	226.74
Nov 02	84%	80.5°	1.28	±13.53%	338.81	63%	N/A	N/A	N/A	324.77	173°	128°	1.24	1.23	230.39
Jan 03	87%	76.9°	1.28	±14.26%	374.9	18%	N/A	N/A	N/A	342.38	173°	128°	1.32	1.25	235.33
Mar 03	85%	78.5°	1.24	±11.86%	401.06	16%	N/A	N/A	N/A	352.27	173°	128°	1.38	1.25	236.62
May 03	92%	75.5°	1.25	±11.97%	375.69	57%	N/A	N/A	N/A	350.27	173°	128°	1.29	1.23	240.05
July 03	88%	81.7°	1.28	±11.81%	322.45	60%	N/A	N/A	N/A	323.01	173°	128°	1.24	1.21	235.31

	Control a = 5 m					Control a = 10 m					Control a = 20 m				
Date	R^2	Az	λ	% aniso	Av ρ_a	R^2	Az	λ	% aniso	Av ρ_a	R^2	Az	λ	% aniso	Av ρ_a
Aug 01	65%	N/A	N/A	N/A	174.03	56%	N/A	N/A	N/A	189.77	85%	10.1°	1.35	±18.76%	181.05
Oct 01	87%	99.5°	1.22	±12.67%	152.4	6%	N/A	N/A	N/A	191.81	90%	6.1°	1.39	±18.15%	183.22
Jan 02	82%	107.8°	1.09	±5.17%	165.18	66%	N/A	N/A	N/A	201.69	80%	179.5°	1.43	±19.68%	190.77
Mar 02	93%	112.3°	1.1	±5.04%	159.73	54%	N/A	N/A	N/A	194.21	91%	6.1°	1.39	±18.38%	183.27

Apr 02	61%	N/A	N/A	N/A	174.25	3%	N/A	N/A	N/A	201.48	90%	5.7°	1.38	±18.13%	186.92
Jul 02	56%	N/A	N/A	N/A	152.4	73%	78.3°	1.06	±3.44%	186.99	90%	9.3°	1.39	±19.19%	181.67
Sep 02	75%	94°	1.18	±9.91%	137.96	67%	N/A	N/A	N/A	179.39	90%	9.1°	1.37	±18.45%	177.33
Nov 02	83%	99.5°	1.12	±7.45%	147.48	33%	N/A	N/A	N/A	188.92	91%	3.0°	1.32	±15.11%	183.81
Jan 03	77%	98.3°	1.14	±10.09%	167.50	70%	156°	1.05	±3.76%	205.5	90%	2.1°	1.41	±18.18%	189.35
Mar 03	83%	105.7°	1.10	±6.56%	192.13	-	-	-	-	218.79	91%	179.7°	1.38	±16.74%	194.10
May 03	85%	118.0°	1.11	±6.09%	171.84	-	-	-	-	212.06	90%	3.5°	1.39	±17.38%	194.96
July 03	61%	N/A	N/A	N/A	151.50	-	-	-	-	192.95	90%	6.5°	1.37	±18.97%	188.01

Key

R^{2} = Reduction in variance

% aniso = Percentage anisotropy

Az = Azimuth of fracture strike

Av ρ_a = Average apparent resistivity (Ω.m)

λ = Coefficient of anisotropy

Note: The strike azimuth is relative to UTM Zone 33 grid north, but is based on a magnetic compass bearing of 230° and an assumed magnetic declination of +3° (E).

6.4.2 Graphical plots of parameters

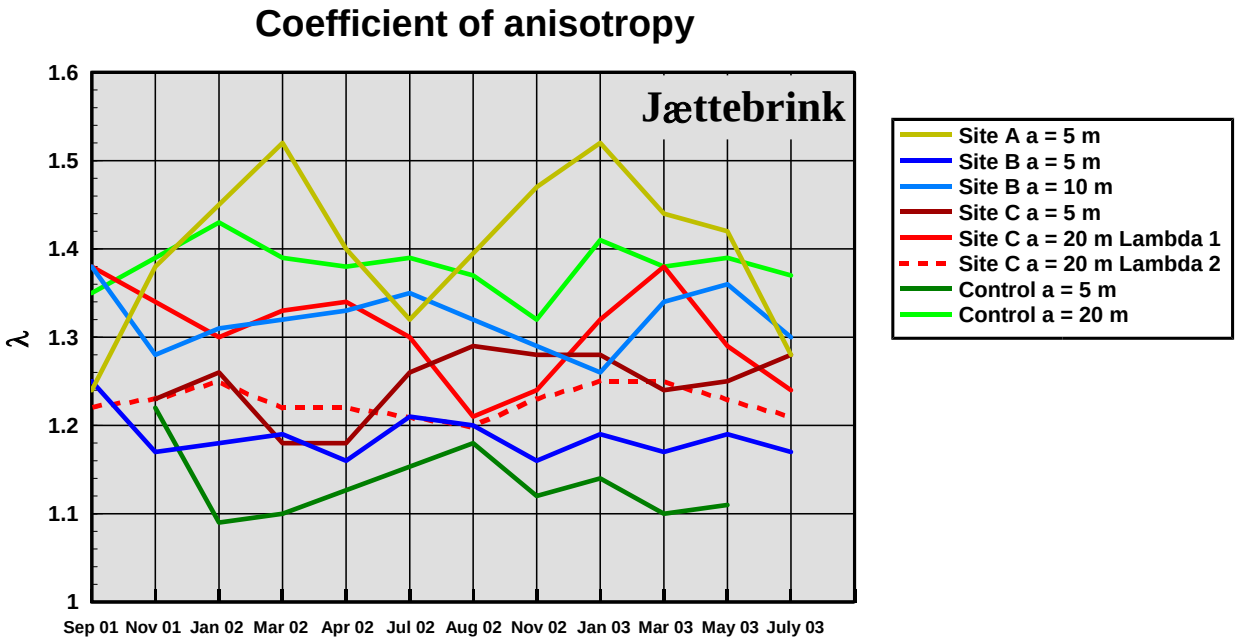

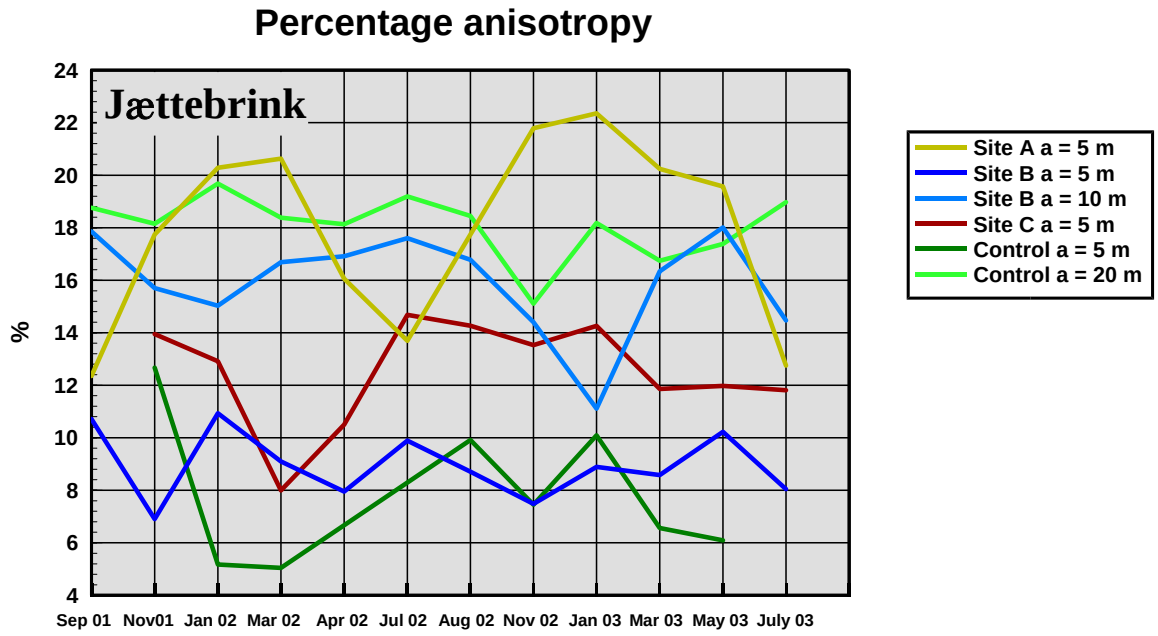

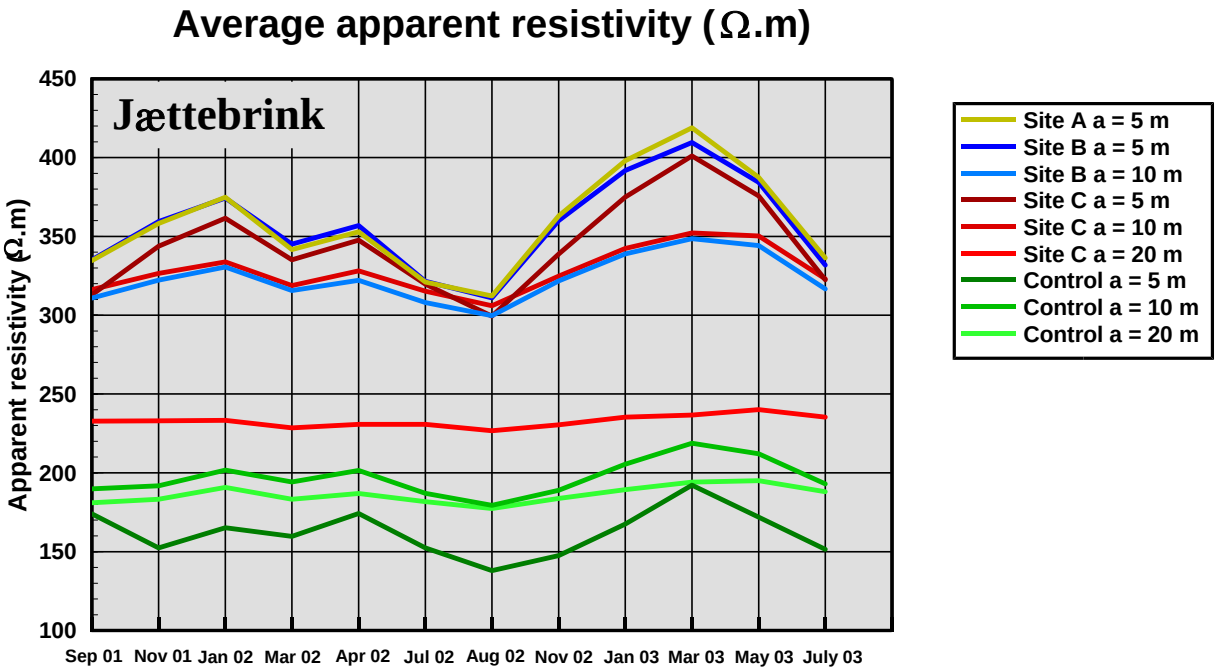

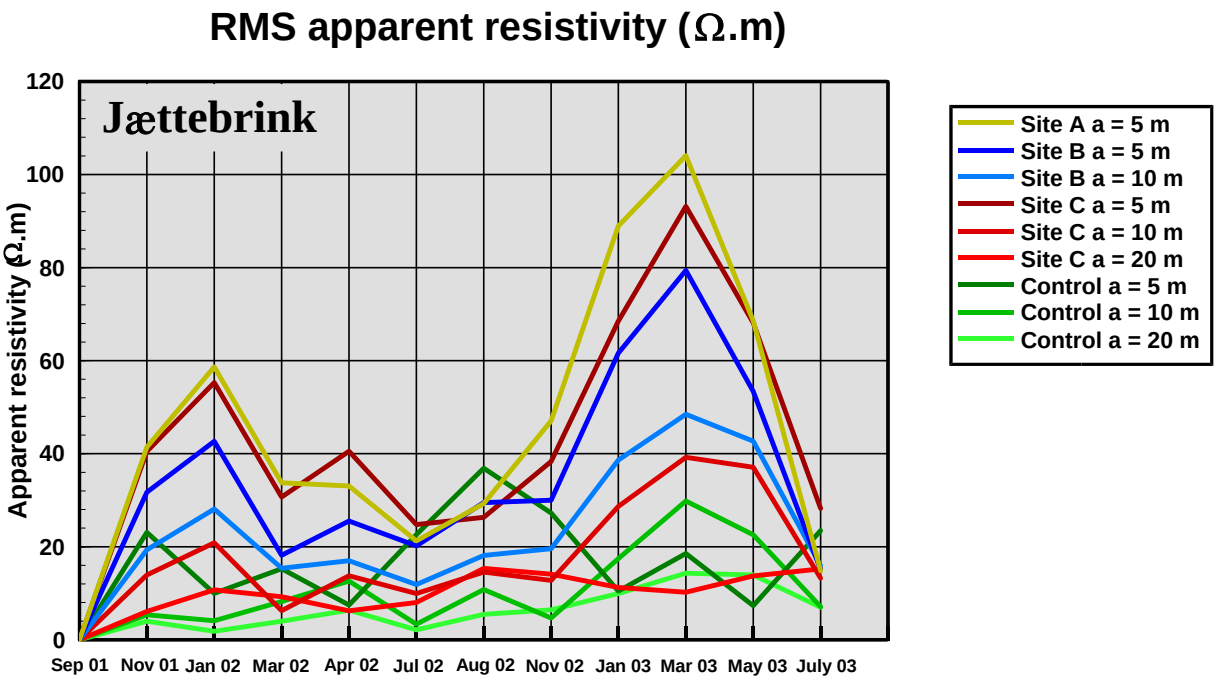

6.4.3 Results summary

Assuming the anisotropy arises from fracturing, the interpreted orientations of the primary fracture sets are as follows.

A, a = 5 m	B, a = 5 m	B, a = 10 m	C, a = 5 m	C, a = 20 m	Control a = 5 m	Control a = 20 m
125°	155°	166°	77°	173° & 128°	104°	5°

Unlike the UK and French research sites there is no clear pattern to the strike azimuths of the fractures. A number of different orientations arise from the sites near the cliff edge; the only cliff parallel azimuth arises from Site A. The most likely tectonic fracture orientation is 5°, measured with a spacing of 20 m at the Control Site. These results are consistent with the geological

mapping that indicates a highly fractured rock mass with many fracture sets at different orientations, but of low persistence.

The quantitative measures of anisotropy do not display any consistent patterns. The Site A values peak in the winter, but this is not shown by the other sites.

The average apparent resistivities are very consistent, with peaks in the winter and troughs in the summer. There is a considerable increase in apparent resistivity towards the cliff edge. The rms apparent resistivities also show peaks in the winter.

6.5 DRONNINGESTOLEN

6.5.1 Tabulated parameters

	Site A a = 5 m					Site B a = 5 m					Site B a = 10 m				
Date	Az_1	Az_2	λ_1	λ_2	Av ρ_a	R^2	Az	λ	% aniso	Av ρ_a	R^2	Az	λ	% aniso	Av ρ_a
Sep 01	98°	53°	1.25	1.22	128.48	93%	50.8°	1.38	±18.29%	131.73	81%	53.8°	1.55	±29.58%	192.2
Nov 01	98°	30.5°	1.19	1.26	135.73	-	-	-	-	-	-	-	-	-	-
Jan 02	98°	45.5°	1.19	1.21	150.52	97%	49.5°	1.33	±13.97%	147.38	81%	44.1°	1.45	±26.01%	209.45
Mar 02	-	23°	-	1.20	123.85	90%	56.5°	1.21	±10.62%	123.79	94%	41.1°	1.46	±20.05%	180.19
Apr 02	-	8°	-	1.14	115.16	86%	58.2°	1.19	±10.37%	117.75	74%	52.7°	1.33	±19.46%	174.81
Jul 02	-	53°	-	1.32	113.18	93%	47.9°	1.32	±15.82%	118.05	79%	59.4°	1.52	±26.11%	176.63
Aug 02	-	53°	-	1.35	113.46	94%	50.3°	1.40	±18.98%	120.53	83%	56.9°	1.62	±29.41%	179.38
Nov 02	98°	45.5°	1.18	1.19	138.03	95%	47.2°	1.30	±13.07%	139.64	86%	53.3°	1.56	±26.91%	198.57
Jan 03	90.5°	45.5°	1.18	1.23	139.64	87%	64.0°	1.25	±14.85%	142.01	85%	56.0°	1.44	±22.74%	201.02
Mar 03	90.5°	38°	1.25	1.26	145.04	94%	69.7°	1.28	±12.96%	149.13	83%	57.1°	1.50	±23.75%	208.36
May 03	83°	53°	1.28	1.26	131.86	97%	55.1°	1.29	±13.23%	135.40	89%	49.1°	1.46	±23.67%	198.28
July 03	98°	45.5°	1.23	1.26	122.97	91%	48.8°	1.41	±18.76%	130.88	81%	59.1°	1.63	±28.83%	191.53

	Control a = 5 m					Control a = 10 m				
Date	R^2	Az	λ	% aniso	Av ρ_a	R^2	Az	λ	% aniso	Av ρ_a
Aug 01	24%	N/A	N/A	N/A	206.03	83%	31.5°	1.22	±13.14%	238.3
Oct 01	67%	N/A	N/A	N/A	202.05	84%	22.9°	1.18	±10.59%	235.92
Jan 02	56%	N/A	N/A	N/A	201.72	77%	20.4°	1.19	±12.13%	238.49
Mar 02	16%	N/A	N/A	N/A	181.76	89%	25.1°	1.22	±11.92%	221.28
Apr 02	70%	N/A	N/A	N/A	186.23	86%	18.4°	1.2	±10.7%	224.03
Jul 02	77%	85.4°	1.07	±5.37%	189.81	78%	25.7°	1.18	±11.76%	228.87
Sep 02	48%	N/A	N/A	N/A	184.58	66%	N/A	N/A	N/A	228.06
Nov 02	83%	130.7°	1.07	±4.58%	193.29	76%	32.5°	1.12	±8.86%	236.06
Jan 03	28%	N/A	N/A	N/A	197.76	81%	20.1°	1.19	±11.32%	241.51
Mar 03	30%	N/A	N/A	N/A	211.84	77%	15.6°	1.19	±11.0%	248.75
May 03	60%	N/A	N/A	N/A	209.92	81%	17.1°	1.20	±11.41%	249.11
July 03	36%	N/A	N/A	N/A	206.03	85%	27.2°	1.16	±9.77%	247.06

Key

R^2 = Reduction in variance

Az = Azimuth of fracture strike

λ = Coefficient of anisotropy

% aniso = Percentage anisotropy

Av ρ_a = Average apparent resistivity (Ω.m)

Note: The strike azimuth is relative to UTM Zone 33 grid north, but is based on a magnetic compass bearing of 230° and an assumed magnetic declination of +3° (E).

6.5.2 Graphical plots of parameters

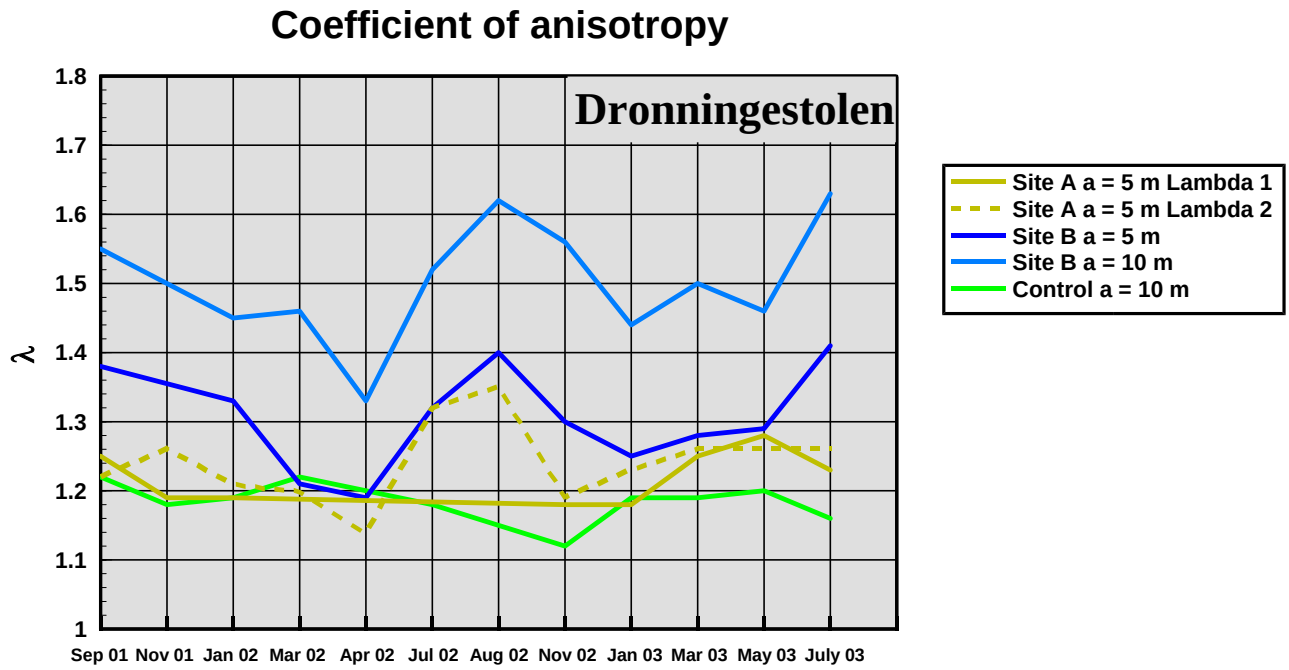

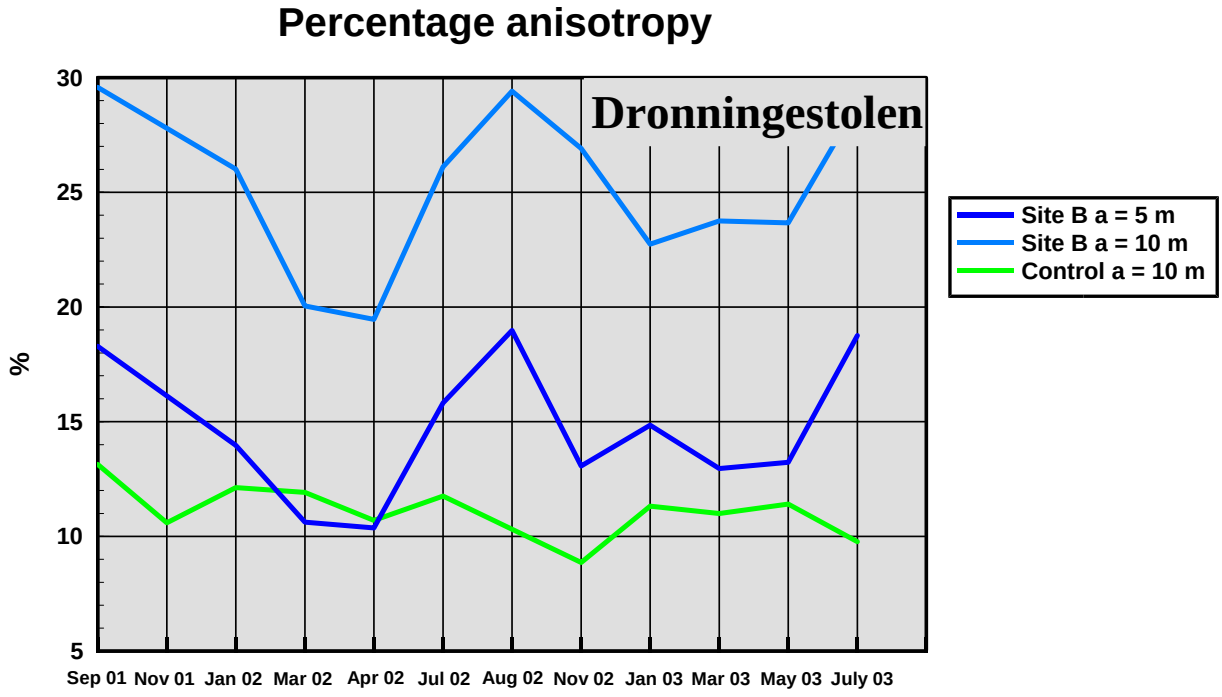

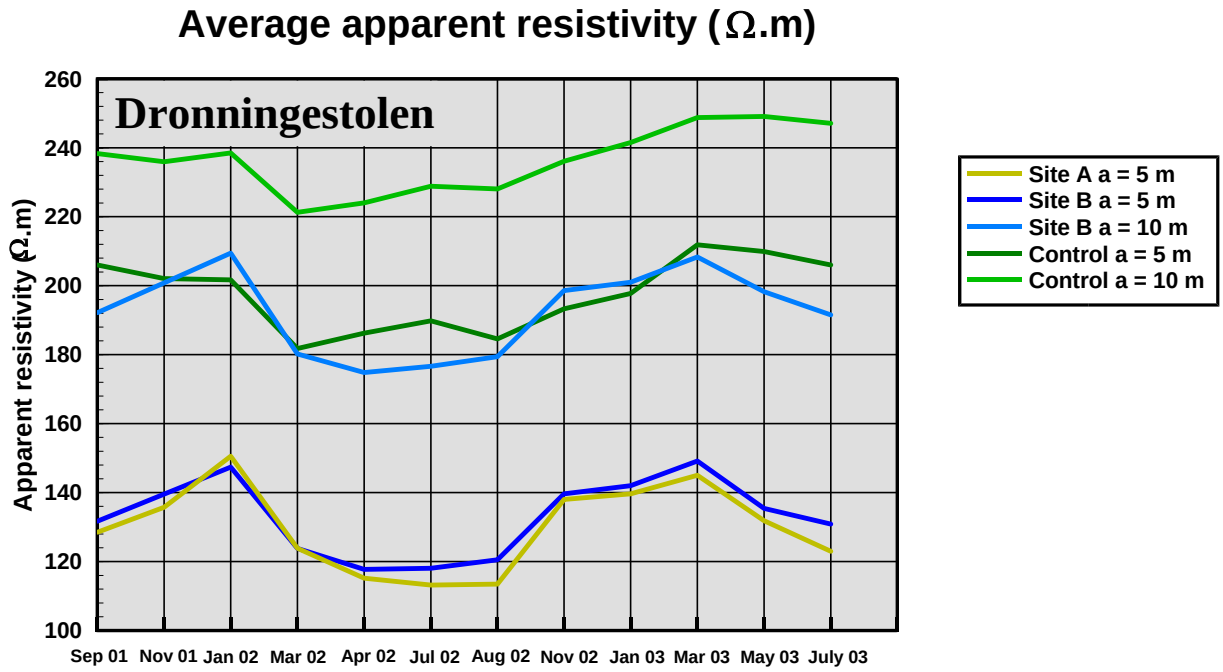

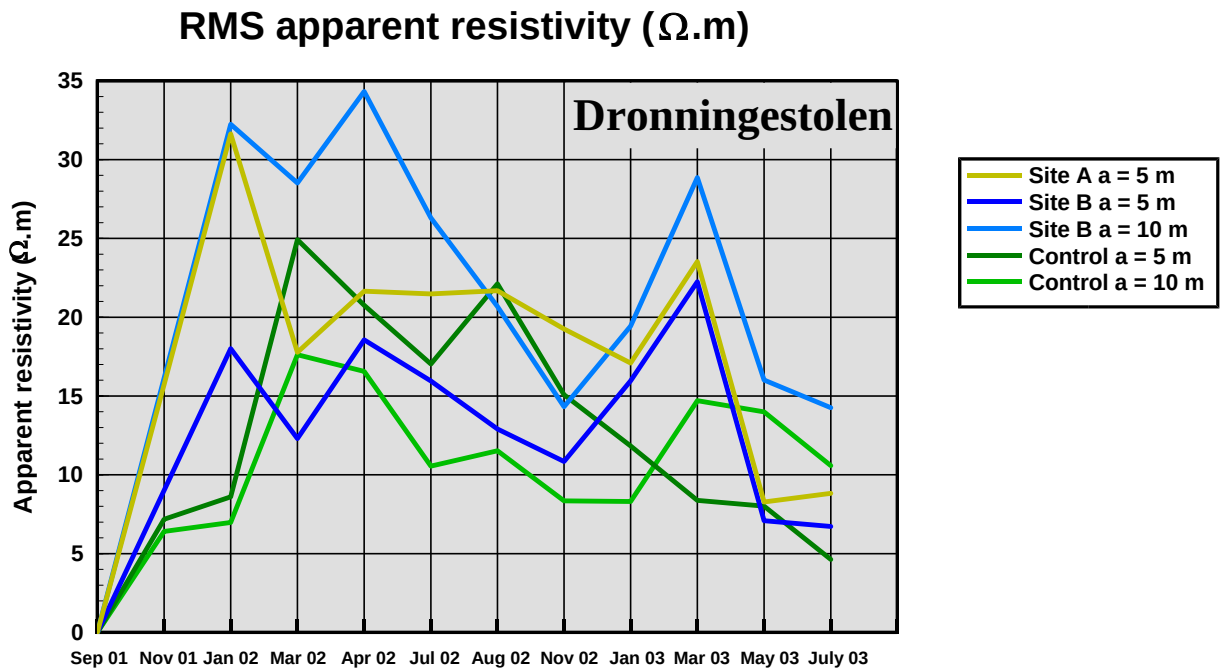

6.5.3 Results summary

If it is assumed that the anisotropy arises from fracturing, the interpreted orientations of the primary fracture sets are as follows.

A, a = 5 m	B, a = 5 m	B, a = 10 m	Control a = 10 m
94° & 41°	54°	53°	23°

A variety of fracture orientations are indicated with the Site B values producing the most consistent result. All of the orientations are at a high angle to the cliff suggesting no cliff parallel fracture set. However, the anisotropy in the ground may not be due to fracturing, but may be

caused by moisture variations in the near surface arising from the trees. The results from Site A were very variable and cannot be relied upon.

The coefficients of anisotropy show a peak in summer with lower values in the winter. The average apparent resistivities display lower values over the summer with peaks in the winter. There is a distinct decrease in resistivity towards the cliff edge. The rms apparent resistivities are more random.

7 Analysis

7.1 NATURE OF THE ANISOTROPY

It is important to establish if the anisotropy is likely to be due to fracturing since there are a number of other ground conditions that generate anisotropy. Two situations need to be distinguished. The first is where apparent resistivity varies with electrode array orientation, but is independent of coordinates (Bolshakov et al., 1997). In this case, the ground is anisotropic and homogeneous. In the second case, apparent resistivity is dependent on both the coordinates and orientation of the electrode array (Habberjam and Watkins, 1967). In the latter case, the ground is anisotropic and inhomogeneous, but the inhomogeneity may vary in a uniform manner and does not therefore manifest itself as random noise. Examples would be a dipping interface between two homogeneous isotropic layers of contrasting resistivity and a gradational change in resistivity (Watson and Barker, 1999).

Busby (2000) has developed a quantitative measure of anisotropy that indicates if the ground is anisotropic and homogeneous. It is based on an offset measurement where the azimuthal measurement is repeated at a distance usually equal to the array spacing. The two offset measurements should be equal since any divergence is related to the inhomogeneity of the rockmass since, by definition, they would be equal over homogeneous ground.

The quantitative measure is based on the divergence between the two measurements, referred to here as D1 and D2. The mean of the $\rho_{D1,D2}$ ellipse defines the radius of the best fitting circle through the data. Hence a measure of the divergence from a circle by the data is the standard deviation of $\rho_{D1,D2}$, i.e. $\sigma(\rho_{D1,D2})$. This can be taken as a measure of anisotropy. Similarly a measure of the dispersion between the two offset measurements is the standard deviation of the absolute value of the difference between ρ_{D1} and ρ_{D2}, i.e., $\sigma(|\rho_{D1} - \rho_{D2}|)$ which has a non-zero mean value. Hence for the rockmass to be considered as anisotropic and homogeneous the anisotropy measure must exceed the measure of dispersion caused by inhomogeneity. This can be expressed by the simple dimensionless quotient:

$$\frac{\sigma(\rho_{D1,D2})}{\sigma(|\rho_{D1} - \rho_{D2}|)}$$

Where $\sigma(\rho_{D1,D2})$ is the standard deviation of the average offset measurement and $\sigma(|\rho_{D1} - \rho_{D2}|)$, or equivalently $\sigma(|\rho_{D2} - \rho_{D1}|)$ is the standard deviation of the absolute difference between the two offset measurements.

An alternative definition of the quotient is

$$\frac{\sigma(\rho_{D1,D2})}{\sqrt{meanvalue[(\rho_{D1} - \rho_{D2})^2]}}$$

where the measure of dispersion in the denominator is the mean deviation of the two offset measurements.

When the two measures are equal, the quotient has a value of 1.0 and the variation due to anisotropy equals that due to inhomogeneity. A value greater than one indicates that the variation due to anisotropy is greater than that due to inhomogeneity, whilst values less than one indicate the reverse.

To investigate the tectonic fracturing an offset square measurement was collected at Birling Gap in July 2002 for a spacing of 20 m. The square was offset by 20 m towards the cliff edge. For the sites near the cliff edge, offset measurements can be approximated from the two a = 5 m measurements at Sites A and B, and the two a = 10 m measurements at Sites B and C. These are offset by 3.53 and 7.07 m respectively. Homogeneity indices have been calculated for all sites based on the measurements taken in July 2002 and are tabulated in Table 2.

Location	Homogeneity index	
	$\frac{\sigma(\rho_{D1,D2})}{\sigma(\lvert\rho_{D1}-\rho_{D2}\rvert)}$	$\frac{\sigma(\rho_{D1,D2})}{\sqrt{meanvalue[(\rho_{D1}-\rho_{D2})^2]}}$
Birling Gap Control, a = 20 m	3.39	1.46
Birling Gap Sites A & B, a = 5 m	3.16	1.34
Birling Gap Sites B & C, a = 10 m	0.86	0.60
Beachy Head Sites A & B, a = 5 m	7.40	4.45
Beachy Head Sites B & C, a = 10 m	0.66	0.42
Mesnil-Val Sites A & B, a = 5 m	1.04	0.67
Mesnil-Val Sites B & C, a = 10 m	1.77	0.89
Jættebrink Sites A & B, a = 5 m	1.46	0.87
Jættebrink Sites B & C, a = 10 m	0.67	0.29
Dronningestolen Sites A & B, a = 5 m	2.38	1.16

Table 2. Homogeneity indices calculated for all five sites from data collected in July 2002.

The lowest values occur for Beachy Head Sites B & C, ‘a’ = 10 m, and Jættebrink Sites B & C, ‘a’ = 10 m where in both cases data considered to be isotropic were collected for Site C, ‘a’ = 10 m. At the Birling Gap Control Site the high homogeneity indices indicate that the anisotropy is not due to a resistivity gradient or a dipping interface. Since thin steeply dipping beds are known not to be present, the most likely explanation for the anisotropy is tectonic fracturing.

Near the cliff edge at Birling Gap the high homogeneity indices also indicate that the anisotropy is due to fracturing that is sub-parallel to the cliff face. Slightly further back from the cliff edge the ground is inhomogeneous and the anisotropy is most likely caused by a resistivity gradient. This may not preclude fracturing since the fracture intensity of the cliff parallel fractures will decrease away from the cliff creating a resistivity gradient. If so, it indicates that the zone of fracturing is quite narrow, around 10 m in width. A similar result is found for Beachy Head where the ground is highly homogeneous near the cliff edge. At Mesnil-Val the two homogeneity indices suggest that the ground can be considered homogeneous if the less stringent quotient, defined by the standard deviation of the average offset measurement and the standard deviation of the absolute difference between the two offset measurements, is applied. Here the homogeneity extends farther back from the cliff suggesting that the zone affected by the cliff parallel fractures is wider, probably around 20 m in width.

The homogeneity indices from Jættebrink, near the cliff edge, also indicate that the ground can only be considered homogeneous if the less stringent criterion is applied. It is likely that the cliff parallel fractures occur in a narrow zone, less than 10 m in width. At Dronningestolen the

homogeneity indices produce high values indicating that the anisotropy is homogeneous and thus most likely indicates a dominant fracture set at a high angle to the cliff face.

7.2 TECTONIC FRACTURING ON THE EAST SUSSEX COAST OF THE UK

The Beachy Head and Birling Gap research sites are only 2.5 km apart and both are sited upon Seaford Chalk. However, the estimated azimuths of the primary tectonic fracture sets are different and the coefficient of anisotropy calculated for Birling Gap is much larger than that for Beachy Head. In order to investigate these large changes, two further sites, along the coast but away from the cliff edge, were also measured between Beachy Head and Birling Gap. These are referred to as Shooters Bottom and Belle Tout and are approximately 0.75 and 2.0 km from Beachy Head. The results for all four sites for a square array spacing of 20 m are summarised in Table 3.

Location	*Co-ordinates (BNG Easting & Northing)*	*Strike of fractures*	*λ*
Beachy Head	558.11 95.29	151°	1.22
Shooters Bottom	557.38 95.36	126°	1.28
Belle Tout	556.06 95.61	123°	1.53
Birling Gap	555.65 95.73	73°	1.96

Table 3. Estimates of the tectonic fracture azimuths and the coefficients of anisotropy from the four sites between Beachy Head and Birling Gap. Values are calculated from the array spacing of 20 m.

These data show a progressive change in strike of the primary fracture set and an increase in the coefficient of anisotropy, from Beachy Head to Birling Gap. The data indicate that the mapped fractures that strike at 150° are the dominant fracture set at Beachy Head and those striking at 70° dominate at Birling Gap. The intermediate fracture strikes at Shooters Bottom and Belle Tout may result from the orientation of greatest fracture connectivity due to the influence of two similar fracture sets. The increase in λ may represent an increase in fracture density (on the scale of the measurement) of the primary fracture set.

7.3 COMPARISONS WITH CLIFF FALLS, ROCK PROPERTY, AND METEOROLOGICAL DATA

This section attempts to interpret the results obtained from the azimuthal apparent resistivity measurements. The two previous sections have examined the anisotropy obtained and have concluded that fracturing plays a major part. Comparisons are now made with other data sets to explain the variations observed.

7.3.1 Mesnil-Val

At Mesnil-Val the anisotropy observed near the cliff edge has been interpreted as a cliff parallel fracture set that may extend up to 20 m from the cliff edge. The Control Site indicates two conjugate tectonic fracture sets of similar intensity striking at 16° and 117° that broadly agree with mapped fracture strikes of 30° and 127°. The coefficient of anisotropy λ, displays strong seasonal variations with peaks in the summer (May to September) and lowest values in the winter. The large magnitude changes in λ at Site A were also apparent at the Control Site, a phenomenon seen only at Mesnil-Val. Electrical resistivity imaging by BRGM has identified an electically conductive feature striking at approximately 20° in the vicinity of the Control Site. Geological mapping suggests that this feature is most probably a clay filled solution feature that follows the fracturing. It may thus partly explain some of the variations observed at the Control Site.

A cliff fall occurred at Mesnil-Val on 23rd June 2002. Calculations made by GEUS from the topographic grid monitoring indicate that approximately 2700 m^3 of chalk dropped from a maximum height of around 50 m. The cliff profile at the western part of the site was substantially altered by the fall, with up to 4 m of the cliff edge being lost. The area of investigation by the azimuthal resistivity measurements was not directly affected by the fall; the closest approach of any electrode to the ground lost was approximately 4 m. There are no indications in the measures of anisotropy or the temporal apparent resistivity data sets of the fall. This implies that a fall outside the area of direct investigation is not detectable with azimuthal apparent resistivity. The implication is that fracture dilatancy is limited to the block of rock constrained by the conjugate fractures and these factures limit the lateral extent of the fall.

BRGM have been collecting meteorological and rock mass data at Mesnil-Val since February 2002. Of interest, are air temperature, rainfall and rock temperature data. Rock temperature data were collected with Humilog sensors that were emplaced in horizontal boreholes in the front face of the cliff. The boreholes were vertically aligned at depths from the cliff top of 15.75 (H1), 24.5 (H2) and 33.25 (H3) m. The sensors were emplaced into the boreholes at horizontal distances from the cliff face of 3 and 6 m. Graphical plots of these meteorological and rock temperature data are shown in Figures 17 and 18.

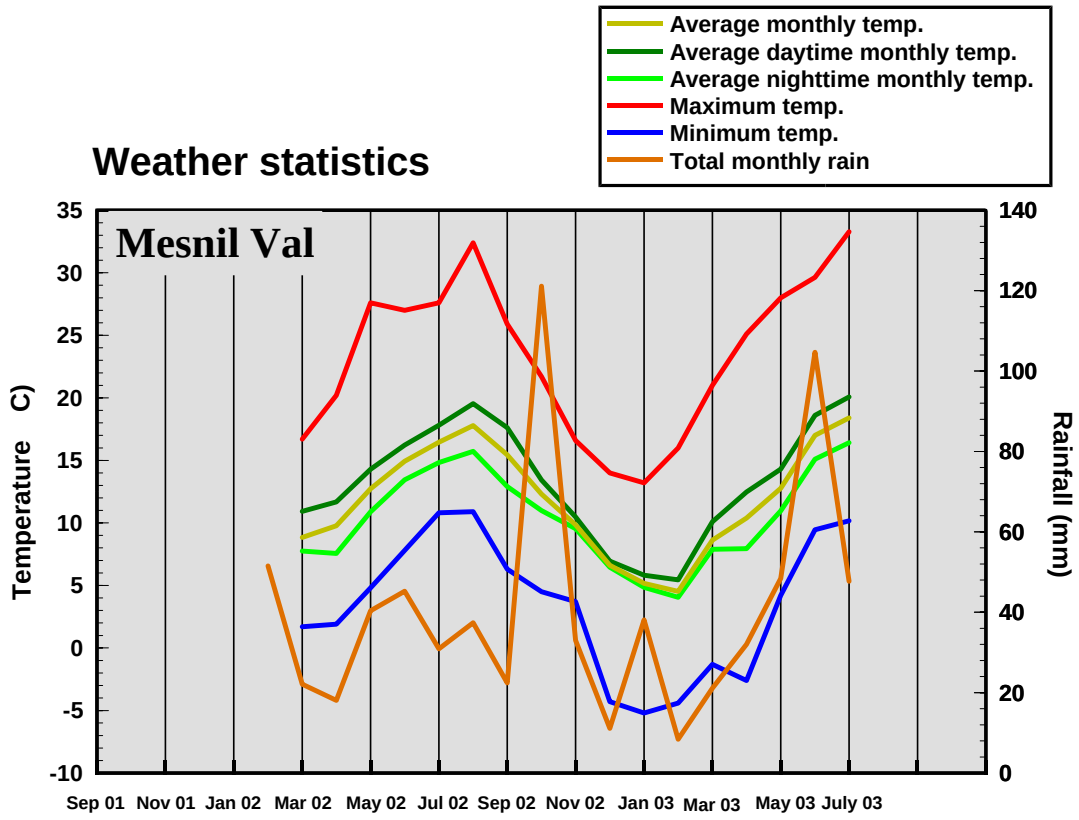

Figure 17. Air temperature and rainfall data from the meteorological station at Mesnil-Val.

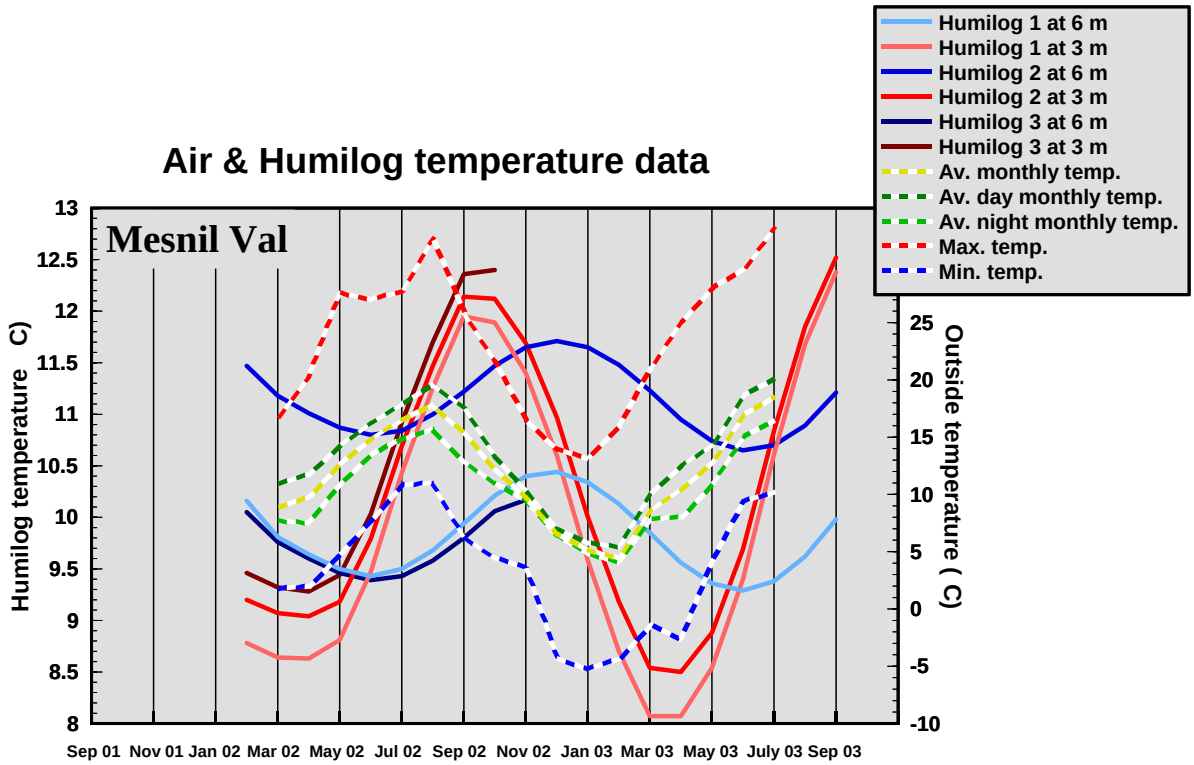

Figure 18. Air temperature and rock temperature data from Mesnil-Val.

Over the period of monitoring, average monthly rainfall has been below average compared to weather statistics from Dieppe. There are two distinct peaks at October 2002 and June 2003. There are no obvious correlations between rainfall and the quantitative measures of anisotropy or the apparent resistivity data.

The outside temperature variations and the Humilog temperatures are clearly linked. It is well known that to depths of around 15 m, rock temperature changes are driven by atmospheric temperatures. There is a phase shift of 1 to 2 months between the temperature variations at the cliff face and those at a depth of 3 m and 4 months between the cliff face and those at a depth of 6 m. From the differences in harmonic amplitude, temperature variations between the three measuring points (the cliff face, 3 m and 6 m), an average thermal transmissivity of 5.98 x 10^{-3} cm^2 s^{-1} has been calculated. This is lower than quoted thermal transmissivities of chalk of around 10.0 x 10^{-3} cm^2 s^{-1}, but the fractured, dryer than average nature of the chalk, would lower the value. Thus this is reasonable evidence to suggest that the thermal variations within the rockmass are being driven by atmospheric temperature variations and not variations in the geothermal gradient.

There is a clear correlation between temperature variations and the quantitative measures of anisotropy. BRGM have installed two extensometers in horizontal boreholes in the cliff face at Mesnil-Val. The extensometers measure the lengthening or shortening of a sliding iron stem in a tube that can be related to the opening or closing of fractures. The extensometers are along the same vertical line as the Humilogs at depths from the cliff top of 12 (Ext 1) and 27.5 (Ext 2) m. Extensometer 1 was placed to a depth of 6 m in the borehole and extensometer 2 to a depth of 4 m. The data record the change in length of the extensometer compared to the length on 1st February 2002. From the graph in Figure 19, there is a clear link between temperature variations and expansion and contraction of the rock mass, although the movements are extremely small. There is a maximum expansion in February and minimum contraction in September. The nature of the coupling between these seasonal variations and the quantitative measures of anisotropy is not clear. It might be expected that an expansion of the rock mass would lead to fracture

dilatancy near the free cliff face that would lead to an associated peak in the measures of anisotropy. However, the reverse is shown by the data, implying that the expansion of the rock mass is taken up by a contraction of the fractures. It is also to be expected that the rock mass will be under a number of stresses due to the phase shift in temperature variations propagating through the chalk. Hence, the peaks in the measures of anisotropy might occur at different times for different array spacings, i.e. the spacing of 20 m is penetrating deeper than that of 5 m. However, this also does not seem to be the case for most of the Mesnil-Val data where the peaks and troughs all occur at the same times.

The average apparent resistivity data show the same trends as the measures of anisotropy with an increase of resistivity towards the cliff edge. However there is a general increase in values over the monitoring period. In contrast the measures of anisotropy and the rock temperature data all show a general decrease over the monitoring period.

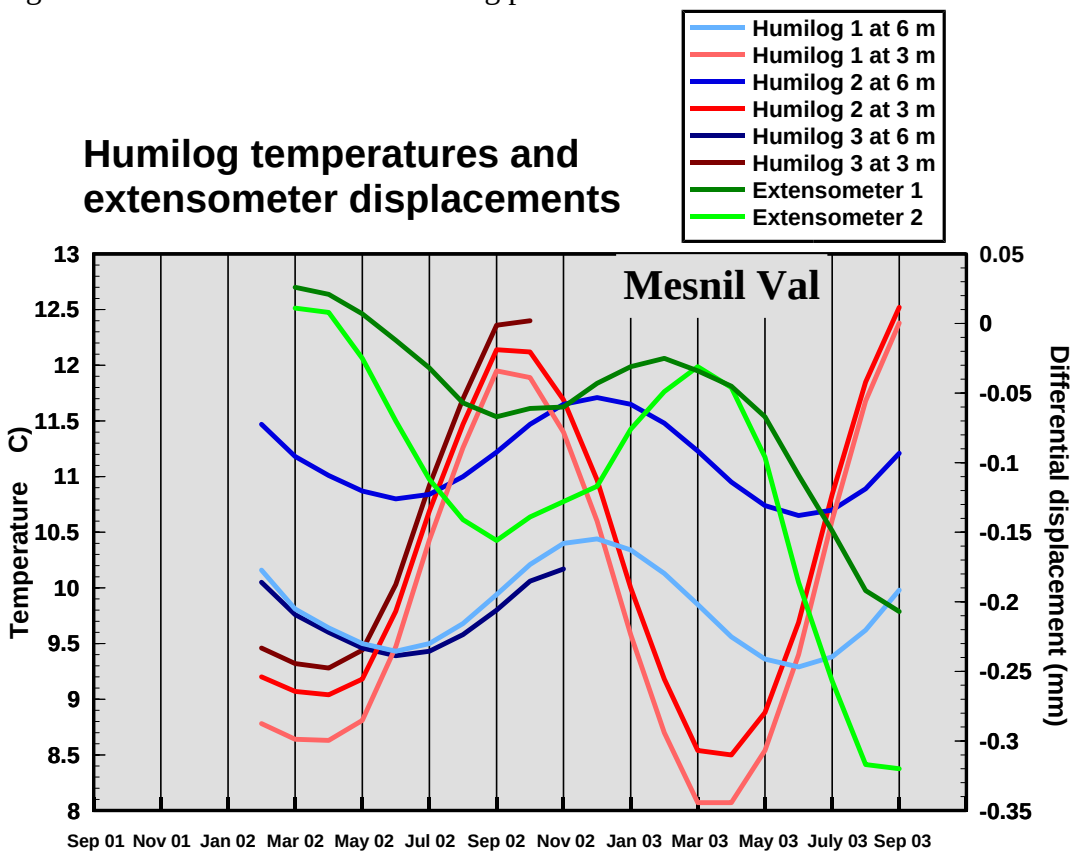

Figure 19. Chart to illustrate the correlation between the expansion and contraction of the rock mass and the Humilog temperatures.

7.3.2 Birling Gap and Beachy Head

The tectonic fracture directions obtained from these two sites have been discussed above in section 7.2. In addition, at both sites, a cliff parallel fracture set has been interpreted near to the cliff edge. This zone is around 10 m in width. The seasonal variations in the coefficient of anisotropy are small at Birling Gap, but large at Beachy Head, with peaks in the summer and troughs in the winter. Average apparent resistivities are constant with time at both sites, but with a low in the winter of 2002/2003. At Beachy Head there is a distinct increase in resistivity towards the cliff edge, whilst at Birling Gap there is no obvious resistivity gradient.

Two small cliff falls occurred at Birling Gap during the period of measurements. The first between March and May 2002 was only discovered when the surveying tapes were laid out and were found to hang over the cliff edge (see Figure 20). Hence, it is estimated that only 1.0 to 1.5 m of the cliff edge was lost and the lateral extent of the fall was probably limited by the fault that cuts the site. However, a large change in the coefficient of anisotropy was seen at Site A with a

smaller, but distinct, change at Site B. This change has been interpreted as resulting from the cliff fall and probably indicates a change in dilatancy within the fracture network. The second fall on 9th January 2003 was also small and occurred outside the zone of resistivity measurements. There is no indication of the fall in the measures of anisotropy. Hence, as at Mesnil-Val, it appears that tectonic fractures may limit the extent of the fracture dilatancy. No cliff falls were reported from Beachy Head.

Figure 20. View of Birling Gap Site A in May 2002. The surveyor's tape hanging over the cliff edge indicates the extent of the cliff lost in the fall.

Figure 21 presents monthly weather statistics from the meteorological station at Eastbourne, the closest to the two sites. Air temperatures peak in mid-summer suggesting that the coefficient of anisotropy peaks, observed in late summer at Beachy Head, are also related to rock temperature. It is unclear why seasonal variations are observed to be small at Birling Gap. The wettest weather occurred in November and December 2002 and was probably responsible for the apparent resistivity low in the winter of 2002/2003.

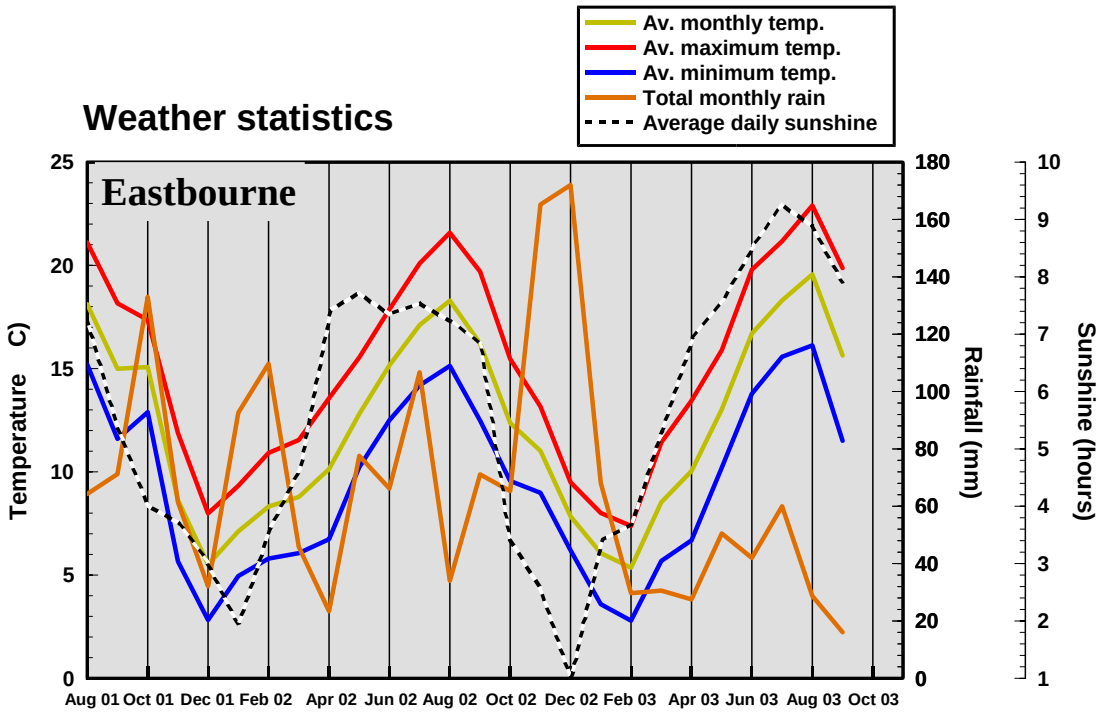

Figure 21. Weather statistics from the meteorological station at Eastbourne.

7.3.3 Jættebrink and Dronningestolen

At Jættebrink, no consistent fracture orientations were interpreted and this appears to be consistent with the mapping that found many fractures of low persistence at different orientations. There are no clear patterns to the measures of anisotropy except at Site A where there are peaks in the winter and lows in the summer, the opposite pattern to Mesnil-Val and Beachy Head. The average apparent resistivity data show peaks in the winter and lows in the summer. At Dronningestolen a number of fracture orientations were interpreted, all at a high angle to the cliff face. Hence there appear to be no cliff parallel fractures although the Site A results were very unreliable, possibly reflecting the influence of the trees. The coefficients of anisotropy display a seasonal variation with highs in the summer and lows in the winter. The average apparent resistivity data also show peaks in the winter and lows in the summer.

Figure 22 shows monthly weather statistics from a local weather station. Air temperature variations again show mid-summer peaks suggesting that variations in the coefficients of anisotropy at Dronningestolen are driven by rock temperature. The unusual pattern from Site A at Jættebrink cannot be explained. The rainfall data shows a clear pattern of wet summers and dry winters that may explain the pattern of average apparent resistivities.

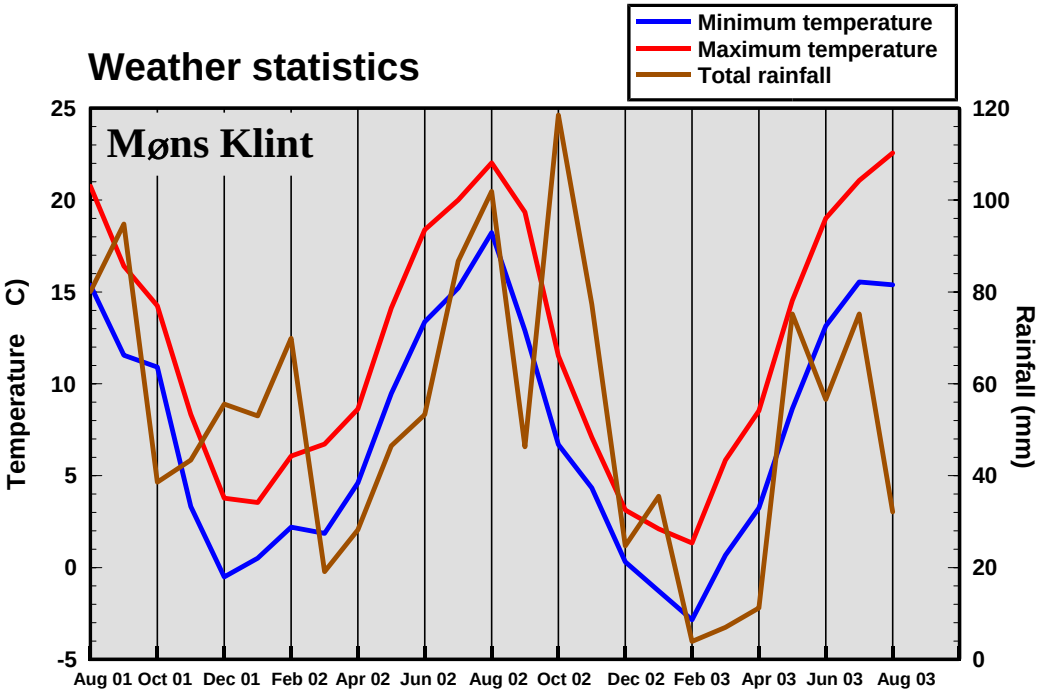

Figure 22. Weather statistics from the meteorological station on the island of Møns.

8 Conclusions

This section briefly lists the main conclusions that can be drawn from the analysis of the azimuthal apparent resistivity data, based on the results for each research site. This is related to the detection of fracture dilatancy and whether the methodology could be applied as an early warning system for impending cliff collapse.

- The azimuthal apparent resistivity measurements have detected anisotropy at all of the research sites. Analysis of offset measurements and comparisons with geological mapping indicate that tectonic fracture orientations are being measured at the Control sites. Towards the cliff edge at the UK and French sites, the analysis indicates a cliff parallel fracture set that is thought to develop in response to the free face at the cliff. This occurs in a zone

adjacent to the cliff edge, 10 to 20 m in width. In Denmark, at Møns Klint, the results are more uncertain, reflecting the glaciotectonised nature of the chalk.

- The 2002 cliff fall at Birling Gap, where ground from within the circle of measurement was lost, produced a large temporal change in the measures of anisotropy. This has been interpreted as a reduction in fracture dilatancy as a result of the cliff fall.
- The Mesnil-Val and Birling Gap 2003 cliff falls did not show temporal changes in the measures of anisotropy. Ground outside of the circle of measurement was lost and it is possible that the tectonic fractures limit the extent of both the fall and the dilating fractures.
- Some sites showed seasonal variations in the measures of anisotropy with peaks in the summer and troughs in the winter. The Mesnil-Val temperature monitoring suggests a correlation between these variations and rock temperature. The thermal transmissivity of the rock is such that the maximum expansion of the rock mass occurs six months after the maximum air temperatures. The data indicate that the expansion leads to fracture contraction with associated minimum values of anisotropy in the winter.
- There is a difference in magnitude of the measures of anisotropy between the Control sites. It is unclear if these magnitude variations can be related to the density of fracturing.
- At Møns Klint there is a correlation between increased rainfall and a reduction in the measured average apparent resistivity. At the other sites, this correlation is less clear, but this may be due to the generally dry conditions. There is an indication of reduced average apparent resistivity after periods of heavy rain.
- The methodology is not yet advanced enough to be able to develop technology for reliable early warning of a cliff fall.
- The next stage of any research would be to install a system for continuous monitoring in order to establish the magnitude of the changes in the measures of anisotropy immediately prior to a cliff fall.
- Overall, the research has been successful in establishing that there are measurable changes in the rock mass prior to a collapse.

9 References

Most of the references listed below are held in the Library of the British Geological Survey at Keyworth, Nottingham. Copies of the references may be purchased from the Library subject to the current copyright legislation.

BARKER, R. D. 1981. The Offset Wenner system of electrical resistivity sounding and its use with a multicore cable. *Geophysical Prospecting*, Vol 29, 128-143.

BUSBY, J. P. 2000. The effectiveness of azimuthal apparent resistivity measurements as a method for determining fracture strike orientations. *Geophysical Prospecting*, Vol. 48, 677-695.

Busby, J. P. 2001. Azimuthal apparent resistivity data collection methodologies for cliff top research. *British Geological Survey Internal Report*, IR/01/169.

BOLSHAKOV D. K., MODIN I. N., PERVAGO E. V. AND SHEVNIN V. A. 1997. Separation of anisotropy and inhomogeneity influence by the spectral analysis of azimuthal resistivity diagrams. *3rd Mtg. Env. and Engin. Geophys. Soc. Eur. Sect., Aarhus, Denmark, Proceedings 1997*, 147-150

BOLSHAKOV, D. K., MODIN, I. N., PERVAGO, E. V. AND SHEVNIN, V. A. 1998. New step in anisotropy studies: Arrow-type arrays. *4th Mtg. Env. and Engin. Geophys. Soc. Eur. Sect., Barcelona, Spain, Proceedings 1998*, 857-860.

HABBERJAM, G. M. AND WATKINS, G. E. 1967. The use of a square configuration in resistivity prospecting. *Geophysical Prospecting*, Vol. 15, 445-467

HART, D. AND RUDMAN, A. J. 1997. Least-squares fit of an ellipse to anisotropic polar data: Application to azimuthal resistivity surveys in Karst regions. *Computers & Geosciences*, Vol. 23, 189-194.

JACKSON, P. D., EARL, S. J. AND REECE, G. J. 2001. 3-D resistivity inversion using 2-D measurements of the electric field. *Geophysical Prospecting*,Vol. 49, 1-15.

LANE, J. W. JR., HAENI, F. P. AND WATSON, W. M. 1995. Use of a square-array direct current resistivity method to detect fractures in crystalline bedrock in New Hampshire. *Ground Water*, Vol. 33, 476-445.

NUNN, K. R., BARKER, R. D. AND BAMFORD, D. 1983. In situ seismic and electrical measurements of fracture anisotropy in the Lincolnshire Chalk. *Quarterly Journal of Engineering Geology, London*, Vol. 16, 187-195.

TAYLOR, R. W. AND FLEMING, A. H. 1988. Characterizing jointed systems by azimuthal resistivity surveys. *Ground Water, Vol.* 26, 464-474.

WATSON K. A. AND BARKER R. D. 1999. Differentiating anisotropy and lateral effects using azimuthal resistivity offset Wenner soundings. *Geophysics*, Vol. 64, 739-745.

WILLIAMSON J. P. 1998. Least-squares fitting of an ellipse to geophysical data derived from azimuthal surveys. *British Geological Survey Regional Geophysics Project Note*, PN/98/9.

APPENDIX

Representative polar plots of the corrected azimuthal apparent resistivity data from some of the research sites are shown in the appendix. For single ellipses, the best fitting ellipse is also shown.

Birling Gap; Control measure; Sixth visit; 2 July 2002

Azimuthal resistivity sounding; Square array

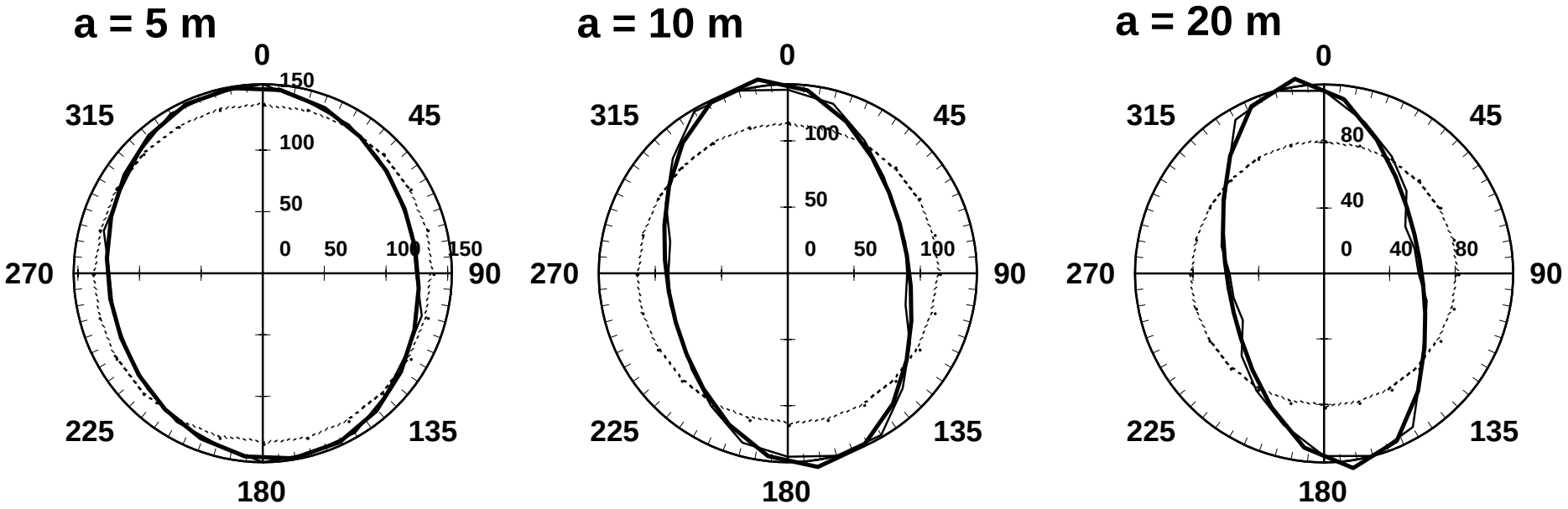

Azimuth of fracture strike = 72.8°
Coefficient of anisotropy = 1.22
Reduction in Variance (R^2) = 97%

Azimuth of fracture strike = 73.4°
Coefficient of anisotropy = 1.63
Reduction in Variance (R^2) = 98%

Azimuth of fracture strike = 73.7°
Coefficient of anisotropy = 2.04
Reduction in Variance (R^2) = 98 %

Measured data (ρ_α) **Best fit ellipse** **Best fit circle**

Polar plot of the measured azimuthal apparent resistivity data, best-fit ellipse and best-fit circle from the control measure at Birling Gap, 6th visit.

Mesnil-Val; Control measure; First visit; 30 August 2001

Azimuthal resistivity sounding; Square array

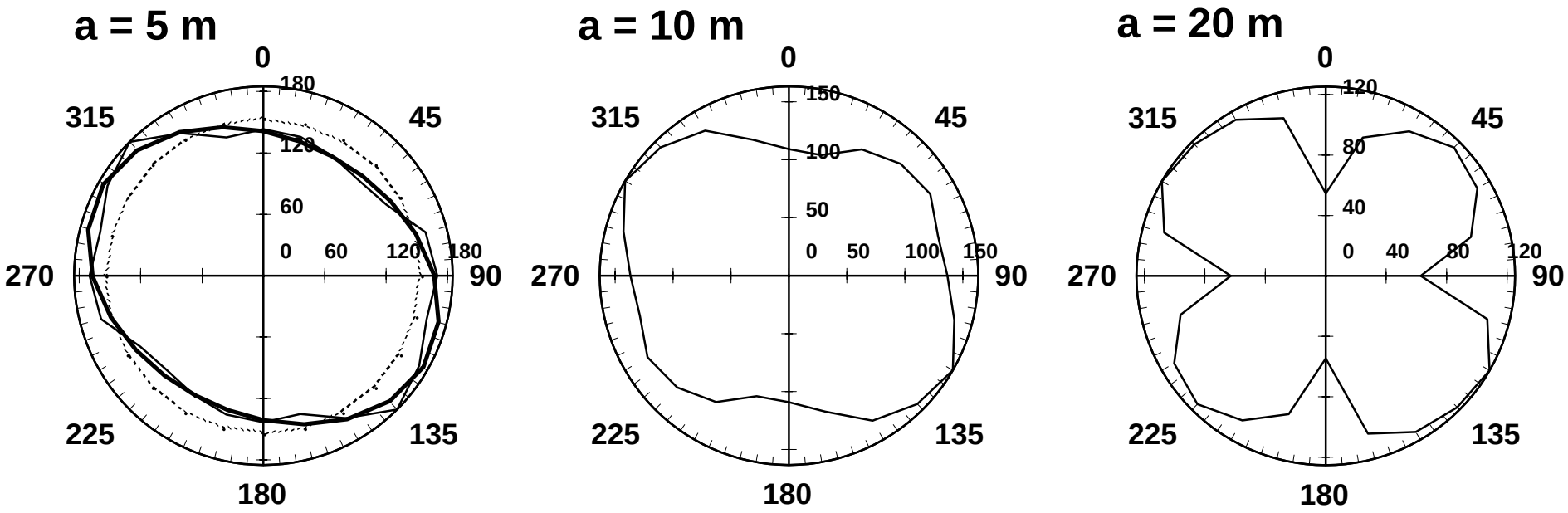

Azimuth of fracture strike = 6.0°
Coefficient of anisotropy = 1.34
Reduction in Variance (R^2) = 85%

Azimuth of fracture strikes = 9 & 129°
Coefficients of anisotropy = 1.52 & 1.29

Azimuth of fracture strikes = 24 & 114°
Coefficients of anisotropy = 2.25 & 2.2

Polar plot of the measured azimuthal apparent resistivity data, best-fit ellipse and best-fit circle from the control measure at Mesnil-Val, 1st visit.

Beachy Head, Sites A & B; Corrected data

Azimuthal resistivity sounding; Square array

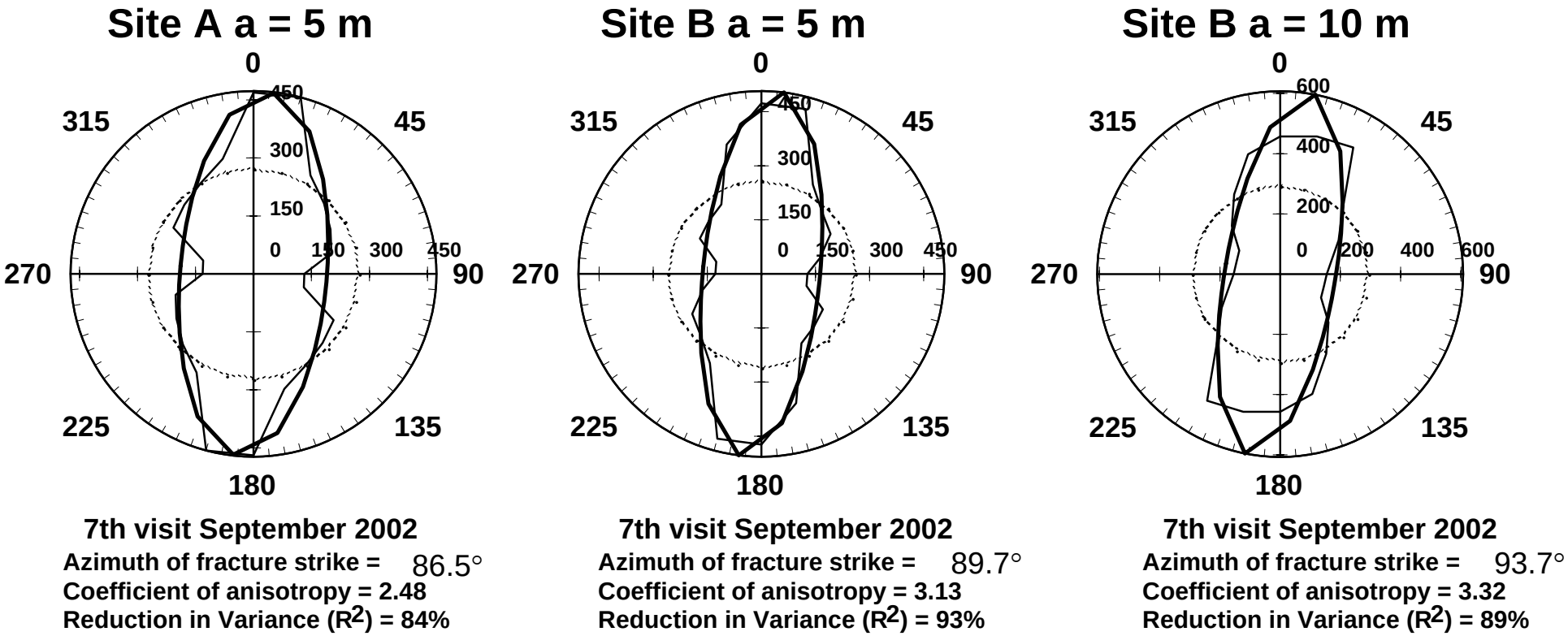

7th visit September 2002
Azimuth of fracture strike = 86.5°
Coefficient of anisotropy = 2.48
Reduction in Variance (R^2) = 84%

7th visit September 2002
Azimuth of fracture strike = 89.7°
Coefficient of anisotropy = 3.13
Reduction in Variance (R^2) = 93%

7th visit September 2002
Azimuth of fracture strike = 93.7°
Coefficient of anisotropy = 3.32
Reduction in Variance (R^2) = 89%

Polar plots of the corrected azimuthal apparent resistivity data, best-fit ellipse and best-fit circle from Sites A & B at Beachy Head.